Cell-Specific Delivery of Diverse Cargos by Bacteriophage MS2 Virus-like Particles

Carlee E. Ashley,[†,○,*] Eric C. Carnes,[‡] Genevieve K. Phillips,[§] Paul N. Durfee,[#] Mekensey D. Buley,[⊥] Christopher A. Lino,[#] David P. Padilla,[†] Brandy Phillips,[§] Mark B. Carter,[§] Cheryl L. Willman,[§,¶] C. Jeffrey Brinker,[†,‡,§,#,▽] Jerri do Carmo Caldeira,[#] Bryce Chackerian,[§,#] Walker Wharton,[§,¶] and David S. Peabody[§,#]

[†]Center for Micro-Engineered Materials, the University of New Mexico, Albuquerque, New Mexico 87131, United States, [‡]Department of Chemical and Nuclear Engineering, the University of New Mexico, Albuquerque, New Mexico 87131, United States, [§]Cancer Research and Treatment Center, the University of New Mexico, Albuquerque, New Mexico 87131, United States, [⊥]Chemical, Biological, and Materials Engineering, University of Oklahoma, Norman, Oklahoma 73109, United States, [¶]School of Medicine, Department of Pathology, the University of New Mexico, Albuquerque, New Mexico 87131, United States, [#]Department of Molecular Genetics and Microbiology, the University of New Mexico, Albuquerque, New Mexico 87131, United States, and [▽]Self-Assembled Materials Department, Sandia National Laboratories, Albuquerque, New Mexico 87185-1349, United States. [○]Present address: Harry S. Truman Post-Doctoral Fellow; Biotechnology and Bioengineering Department, Sandia National Laboratories, Livermore, California 94551, United States.

ABSTRACT Virus-like particles (VLPs) of bacteriophage MS2 possess numerous features that make them well-suited for use in targeted delivery of therapeutic and imaging agents. MS2 VLPs can be rapidly produced in large quantities using *in vivo* or *in vitro* synthesis techniques. Their capsids can be modified in precise locations *via* genetic insertion or chemical conjugation, facilitating the multivalent display of targeting ligands. MS2 VLPs also self-assemble in the presence of nucleic acids to specifically encapsidate siRNA and RNA-modified cargos. Here we report the use of MS2 VLPs to selectively deliver nanoparticles, chemotherapeutic drugs, siRNA cocktails, and protein toxins to human hepatocellular carcinoma (HCC). MS2 VLPs modified with a peptide (SP94) that binds HCC exhibit a 10^4-fold higher avidity for HCC than for hepatocytes, endothelial cells, monocytes, or lymphocytes and can deliver high concentrations of encapsidated cargo to the cytosol of HCC cells. SP94-targeted VLPs loaded with doxorubicin, cisplatin, and 5-fluorouracil selectively kill the HCC cell line, Hep3B, at drug concentrations <1 nM, while SP94-targeted VLPs that encapsidate a siRNA cocktail, which silences expression of cyclin family members, induce growth arrest and apoptosis of Hep3B at siRNA concentrations <150 pM. Impressively, MS2 VLPs, when loaded with ricin toxin A-chain (RTA) and modified to codisplay the SP94 targeting peptide and a histidine-rich fusogenic peptide (H5WYG) that promotes endosomal escape, kill virtually the entire population of Hep3B cells at an RTA concentration of 100 fM without affecting the viability of control cells. Our results demonstrate that MS2 VLPs, because of their tolerance of multivalent peptide display and their ability to specifically encapsidate a variety of chemically disparate cargos, induce selective cytotoxicity of cancer *in vitro* and represent a significant improvement in the characteristics of VLP-based delivery systems.

KEYWORDS: virus-like particles · multivalent peptide display · targeted drug delivery · cancer · nanoparticle · nanocarrier

Despite numerous advances over the past several decades, effective cancer chemotherapy remains challenging. The generalized toxicity of many drugs makes it difficult to achieve therapeutic concentrations without severe systemic side effects. Nanocarriers are being developed that address these issues by selectively delivering drugs to tumor sites. Some designs take advantage of the enhanced permeability of vasculature in the tumor vicinity to promote passive accumulation of drug nanocarriers that are too large to otherwise leave the circulation. Others seek to endow a nanocarrier with the added ability to specifically bind receptor molecules differentially expressed on the surfaces of tumor cells, in the hope that the particle will be internalized and release its contents in a cell-specific manner.

The use of nanoparticles in passive and targeted drug delivery has a relatively long history: the first clinical trials were initiated several decades ago. Since then, nanocarriers composed of synthetic polymers, liposomes, and dendrimers have been investigated, and a few have found clinical applications (see Peer *et al.*[1] for a recent review). Considerably less effort has been invested in the development of vehicles based on virus-like particles (VLPs), even though they possess several features that make them attractive as potential nanocarriers. Here we describe a nanocarrier based on RNA bacteriophage MS2, the VLPs of which self-assemble from 180 copies of a single coat protein (13.7 kDa) into a monodisperse, 27.5-nm icosahedral capsid. The periodicity of the capsid, the presence of surface-accessible amino acids with reactive moieties (*e.g.*, lysine and glutamic acid residues), and the tolerance of a single-chain version of the coat protein dimer to diverse peptide insertions[2] enable dense, repetitive display of targeting peptides either by chemical conjugation or genetic insertion, and display of aptamers, vitamins, glycoproteins, *etc.* by chemical conjugation.[3−9] MS2 VLPs, furthermore, possess a relatively large

* Address correspondence to ceashle@sandia.gov, dpeabody@salud.unm.edu.

Received for review April 16, 2011 and accepted May 26, 2011.

Published online May 26, 2011
10.1021/nn201397z

interior volume that can be loaded with a variety of materials using several approaches.[4,6,8,9] In particular, the ability of MS2 coat protein to spontaneously assemble in the presence of nucleic acids allows the particle to be loaded with therapeutic RNAs or with RNA-conjugated drugs and imaging agents. *In vitro* assembly of VLPs from isolated subunits is most effectively stimulated by a 19-nucleotide RNA stem-loop that specifically interacts with coat protein and normally mediates encapsidation of the viral genome and translational repression of viral replicase synthesis.[7,10,11] Conjugation of this so-called *pac* site to a non-nucleic acid molecule (*e.g.*, a protein) causes the molecule to be packaged within the capsid.[7,8] Coat protein also efficiently encapsidates other types of RNA, making MS2 VLPs readily adaptable to packaging RNAs with therapeutic potential (*e.g.*, siRNA).[11] MS2 VLPs are, additionally, biocompatible, biodegradable, stable under a variety of temperature, pH, and solvent conditions, and easily synthesized and purified in relatively large quantities.[12] Importantly, Peabody, *et al.* recently reported the use of MS2 VLPs as a platform for random peptide display and affinity selection,[2,13] raising the possibility that a single particle can be used both for identification of cell-targeting peptides and for specific delivery of cargo.

Here we report the delivery of several chemically diverse therapeutic and imaging agents to human hepatocellular carcinoma (HCC) using MS2 VLPs modified with high densities of a targeting peptide (SP94) that binds to HCC. The SP94 peptide was previously identified by affinity selection from a phage display library using HCC targets.[14] The possibility of its chemical conjugation to MS2 VLPs provided a convenient means to test the general suitability of the particles for cell-specific delivery. We loaded MS2 VLPs with a variety of cargo molecules using an *in vitro* assembly reaction, modified the resulting particles with SP94, and tested their ability to deliver the various cargo molecules to HCC in culture.

RESULTS

RNA-Driven Assembly of MS2 Coat Protein Enables Encapsidation of Therapeutic and Imaging Agents within VLPs. The techniques we used to encapsidate therapeutic molecules (chemotherapy drugs, siRNA, and ricin toxin A-chain) and an imaging agent (water-soluble CdSe/ZnS quantum dots) within MS2 VLPs are detailed in the Methods section. To summarize, we first conjugated quantum dots, drugs, and ricin toxin A-chain to *pac* site RNA using an appropriate cross-linker. Molar ratios of cargo molecules to *pac* site RNA were determined to be: 1:80 for Qdot 585 ITK amino(PEG) quantum dots, 0.9:1 for doxorubicin (DOX), 1.1:1 for cisplatin, 3:1 for 5-fluorouracil (5-FU), and 1:1 for ricin toxin A-chain (RTA). We then added cargo-*pac* site conjugates to dimerized coat protein, obtained *via* disassembly of MS2 (or Qβ) virions. Buffered, RNA-modified cargos, as well as siRNA in the absence of the *pac* site, drive *in vitro* assembly of VLPs with cargo encapsulated in the interior volume of the 27.5-nm capsid. After removal of excess coat protein and unencapsidated cargos, the exterior VLP surface was modified with an HCC-specific peptide (SP94, H_2N-SFSIIHTPILPL-COOH[14]), a fusogenic peptide (H5WYG, H_2N-GLFHAIAHFIHGGWHGLIHGWYG-COOH[15]), and PEG-1000. Electron microscopy demonstrates that the resulting particles have morphologies indistinguishable from that of wild-type phage; see Figure 1 for a representative electron micrograph of siRNA-loaded VLPs. Furthermore, the relative concentrations of cargo molecules and coat protein in populations of VLPs loaded with drugs, siRNA, or RTA indicate that nearly 100% of fully assembled VLPs contain encapsidated cargo. VLPs that encapsidate CdSe/ZnS quantum dots are the exception: each VLP encapsidates an average of one quantum dot, but ~40% of VLPs in the population are "empty" (see Figure 1 for a schematic depiction of the described process).

SP94-Targeted, Cargo-Loaded VLPs are Selectively Endocytosed by HCC. To determine whether SP94-targeted VLPs are capable of selectively delivering to HCC the therapeutic and imaging agents described above, we prepared a cocktail of particles, each individually loaded with (i) ricin toxin A-chain modified with an Alexa Fluor 488-labeled *pac* site, (ii) *pac* site-modified Qdot 585 ITK amino(PEG) quantum dots, (iii) *pac* site-modified doxorubicin, which is naturally fluorescent, or (iv) Alexa Fluor 647-labeled siRNA. Assembled VLPs were extensively purified using size-exclusion chromatography, chemically conjugated with SP94 at an approximate density of 60 peptides per VLP, fluorescently labeled with Alexa Fluor 532 (Figure 2A) or Alexa Fluor 555 (Figures 2B, 2C, 3, and 4), and incubated with the HCC cell line, Hep3B, for 15−60 min at 37 °C. Since each of the four cargos, as well as the Alexa Fluor 532-labeled capsid, possessed unique spectral characteristics, we were able to individually track them using hyperspectral confocal fluorescence microscopy. Figure 2A indicates that SP94-targeted VLPs can efficiently deliver drugs, siRNA, protein toxins, and quantum dots to HCC, while the representative confocal fluorescence microscopy images shown in Figure 2B,C demonstrate that SP94-targeted VLPs are rapidly internalized by HCC ($t_{1/2}$ = 6 min, as determined by time-course experiments) but show minimal surface binding and no internalization when exposed to normal hepatocytes. We employed flow cytometry to quantify the average number of SP94-targeted VLPs that are internalized by 1×10^6 cells within 1 h at 37 °C and found that each Hep3B cell internalizes an average of 1459 ± 89 VLPs, while each hepatocyte internalizes an average of only 28 ± 19 VLPs; PEGylating the capsid of

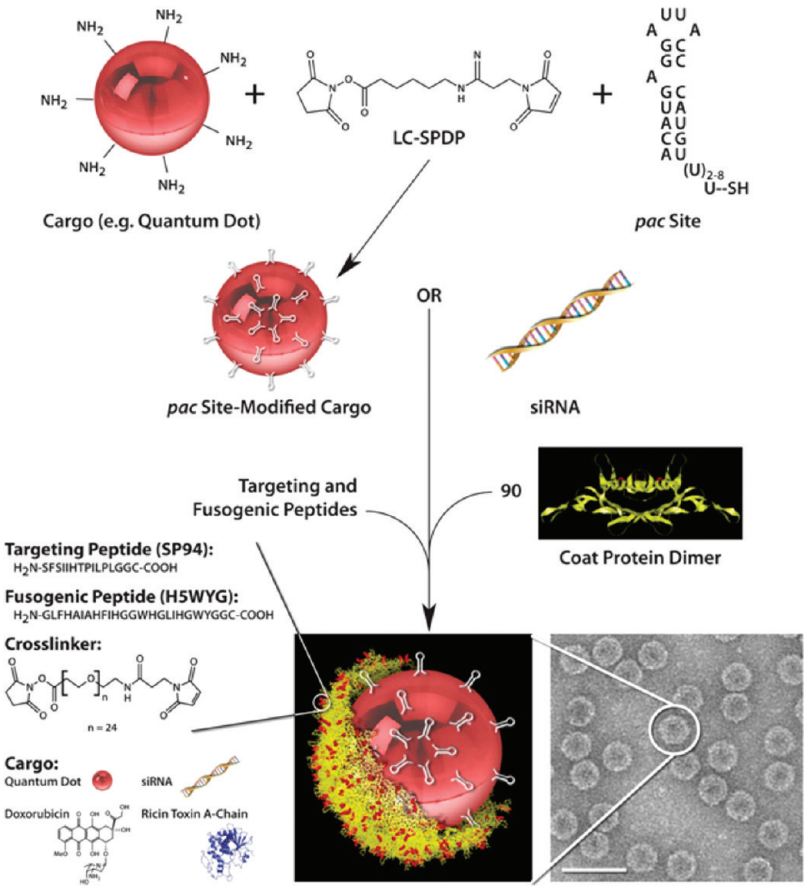

Figure 1. Schematic depicting the process used to synthesize HCC-specific MS2 VLPs that encapsidate chemically disparate therapeutic and imaging agents. Nanoparticles (*e.g.*, quantum dots), protein toxins (*e.g.*, ricin toxin A-chain), and drugs (*e.g.*, doxorubicin) are first conjugated to the *pac* site using an appropriate cross-linker; for example, quantum dots encapsulated within an amine-terminated PEG layer are linked to a derivative of the *pac* site that contains a 3′ uracil spacer and sulfhydryl group using the amine-to-sulfhydryl cross-linker, LC-SPDP. Ninety coat protein dimers then self-assemble around RNA-modified cargo to form the 27.5-nm capsid. siRNA molecules drive capsid reassembly in the absence of the *pac* site and become incorporated within VLPs at an average concentration of ~85 siRNAs per particle; the yield of fully reassembled, siRNA-loaded capsids is depicted in the TEM image (scale bar = 50 nm). Cargo-loaded VLPs can be further modified with targeting peptides to promote selective internalization by cancer cells, with fusogenic peptides to promote endosomal escape of internalized VLPs, and with PEG to reduce nonspecific interactions and mitigate the humoral immune response against coat protein. Peptides synthesized with a C-terminal cysteine residue are linked to lysine residues (red) on the exterior capsid surface (yellow) *via* a heterobifunctional cross-linker with a PEG spacer arm.

SP94-targeted VLPs reduces non-specific uptake by hepatocytes to levels that are not detectable. The VLP capsid was labeled with pHrodo (a pH-sensitive red fluorophore, the emission of which increases dramatically at pH ≤ 6.0) in these experiments to ensure that surface-bound VLPs were excluded. We also quantified the degree to which various surface modifications alter internalization efficacy and found negligible uptake of the following VLPs by Hep3B and hepatocytes: (1) VLPs modified with ~60 copies of an irrelevant peptide (see discussion of the "control" peptide in the next section); (2) VLPs modified with ~75 copies of a histidine-rich fusogenic peptide (see discussion of the "H5WYG" peptide below); (3) VLPs modified with ~145 molecules of PEG-1000; and (4) unmodified VLPs. We, furthermore, observed little difference between the uptake of VLPs that were surface-modified with Alexa Fluor 555 and VLPs that encapsidated Alexa Fluor 555-labeled tRNA, which indicates that the fluorescent molecules we used to track SP94-targeted VLPs do not themselves promote internalization (data not shown).

As is evident in Figure 2A,B SP94-targeted VLPs have a punctate appearance within HCC, which indicates that internalization occurs *via* an endocytotic pathway. Further evidence is provided by the fact that SP94-targeted VLPs are largely colocalized with markers for early (Rab5) and late (Rab7) endosomes (data not shown). Fluorescence colocalization experiments demonstrate that SP94-targeted VLPs are directed to lysosomes upon endocytosis by HCC, as evidenced by the positive Pearson's correlation coefficient (*r*) between SP94-targeted VLPs and lysosomal-associated membrane protein 1 (LAMP-1), as well as the near-zero *r*-value between SP94-targeted VLPs and Rab11a, a

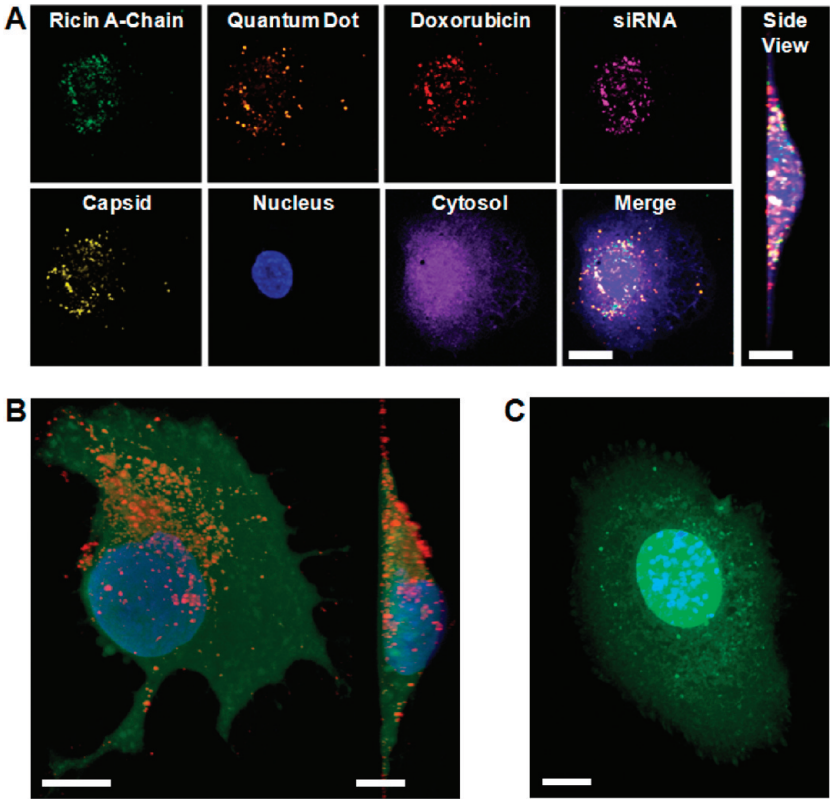

Figure 2. SP94-targeted MS2 VLPs can selectively deliver disparate therapeutic and imaging agents to human HCC. (A) Hyperspectral confocal fluorescence image demonstrating that SP94-targeted VLPs (labeled with Alexa Fluor 532) can simultaneously deliver ricin toxin A-chain (labeled with Alexa Fluor 488), quantum dots (Qdot 585 ITK amino(PEG)), doxorubicin (naturally emits at 560−590 nm), and siRNA (labeled with Alexa Fluor 647) to Hep3B. Cells were labeled with a blue fluorescent nuclear stain (Hoechst 33342) and a purple fluorescent cytosolic stain (CellTracker Violet BMQC). Scale bars = 20 μm. (B and C) Confocal fluorescence microscopy images demonstrating that SP94-targeted VLPs (red) are internalized by Hep3B (B) but not by hepatocytes (C). VLPs were labeled with Alexa Fluor 555. Cells were labeled with Hoechst 33342 and a green fluorescent cytosolic stain (CellTracker Green CMDFA). Scale bars = 10 μm. VLPs were modified with an average of 60 SP94 peptides/particle and were incubated with cells for 30 min at 37 °C in all experiments.

marker for recycling endosomes (Figure 3). Since some therapeutic molecules (*e.g.*, siRNA and protein toxins) are expected to be susceptible to lysosomal degradation, we anticipated the need to promote endosomal escape by further modifying VLPs with a histidine-rich fusogenic peptide (H5WYG) that becomes protonated upon acidification (pK_a = 6.0) and induces osmotic swelling and endosomal membrane destabilization. As demonstrated by Figure 4, VLPs that codisplay the SP94 and H5WYG peptides become dispersed in the cytosol of HCC cells within 1 h of endocytosis, while VLPs that display the SP94 peptide alone remain in endosomes. As demonstrated below, cytosolic dispersion of VLPs and their encapsidated cargos is critical to retain the activity of siRNA and ricin toxin A-chain.

Multivalent Display of Targeting Peptides Enhances the Avidity of MS2 VLPs for HCC. Multivalent display of targeting ligands is known to promote high avidity interactions between nanoparticles and target cells.[6,16−18] To determine the minimum peptide density necessary to promote maximum avidity for HCC, we conjugated various densities of SP94 to the surface of MS2 VLPs using an extended-length, heterobifunctional cross-linker, $SM(PEG)_{24}$; under the conditions described in the Methods section, each VLP can be modified with a maximum of 246 ± 9 (mean ± s.d.) peptides, and peptide density can be reduced in a precise manner by altering the reaction stoichiometry, time, and/or temperature. We then fluorescently labeled SP94-targeted VLPs and employed flow cytometry to quantify their avidity for various HCC cell lines (Hep3B, PLC/PRF/5, and HepG2), as well as untransformed hepatocytes and other control cells (endothelial cells, mononuclear cells, and lymphocytes). Figure 5A shows typical saturation binding curves (after subtraction of non-specific binding), which demonstrate that VLPs bearing ~60 copies of the SP94 peptide bind to Hep3B in a concentration-dependent fashion but show minimal binding to normal hepatocytes, even at high VLP concentrations. To directly compare the avidities of targeted and nontargeted VLPs for various cell lines, we used saturation binding curves to calculate apparent dissociation constants (K_d values), which are a measure of specific surface binding and are inversely

related to avidity (i.e., low dissociation constants are indicative of high affinity or avidity). As demonstrated by Figure 5B, the avidity of MS2 VLPs for HCC is strongly dependent on the density of targeting peptides displayed on the capsid surface, as well as (to a lesser extent) the inherent affinity of the targeting peptide for HCC. K_d values of SP94-targeted VLPs for Hep3B remain essentially constant when they display between ~60 and ~240 peptides/particle. As density decreases to ~30 peptides/particle, however, the avidity of SP94-targeted VLPs for Hep3B starts to decline (*i.e.*, K_d values start to increase). K_d values of MS2 VLPs modified with a second HCC-specific peptide (SP88, H_2N-ELMNPLLPFIQPGGC−COOH[14]) also decrease with increasing peptide density, but higher densities are necessary to achieve comparable avidity, presumably due to the peptide's lower intrinsic affinity for Hep3B (K_d = 489 ± 31.4 nM for monovalent SP88 *versus* 211 ± 12.2 nM for monovalent SP94). Importantly, control experiments demonstrate that SP94-targeted VLPs bind selectively to several HCC cell lines over hepatocytes and other control cells. As shown in Figure 5C, MS2 VLPs decorated with ~60 copies of SP94 have a 10^4-fold higher avidity for Hep3B, PLC/PRF/5, and HepG2 than for human hepatocytes, endothelial cells (HUVECs), and immune cells (peripheral blood mononuclear cells (PBMCs), B-lymphocytes, and T-lymphocytes). Furthermore, SP94-targeted VLPs have a 6000-fold higher avidity for Hep3B than VLPs bearing ~60 copies of an irrelevant peptide ("Control Peptide", H_2N-FPWFPLPSPYGNGGC-COOH[14]) and a 45,000-fold higher avidity for Hep3B than unmodified VLPs, both of which demonstrate that the SP94 peptide promotes specific binding to HCC.

It is important to note that the VLPs used for targeted delivery of therapeutic molecules were routinely PEGylated in the expectation that, when they are eventually tested *in vivo*, this should minimize proteolytic degradation, reduce the anti-VLP humoral immune

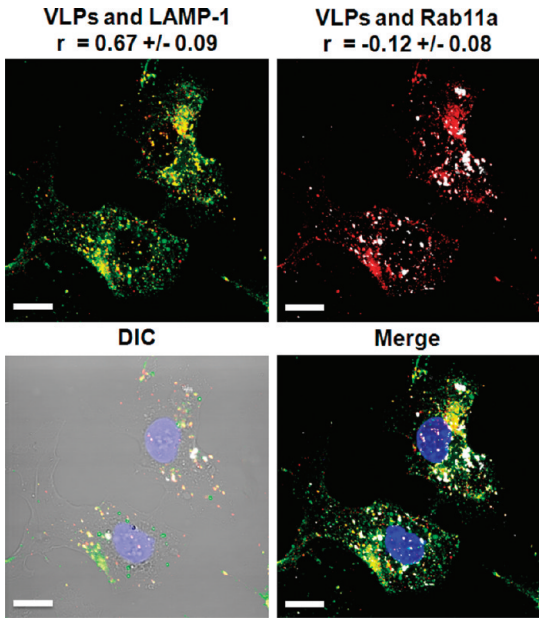

Figure 3. SP94-targeted VLPs are directed to lysosomes upon endocytosis by HCC. Confocal fluorescence microscopy image demonstrating colocalization between Alexa Fluor 555-labeled VLPs (red) and an Alexa Fluor 488-labeled marker for lysosomes (LAMP-1, green) but not between VLPs and an Alexa Fluor 647-labeled marker for recycling endosomes (Rab11a, white). SlideBook software was used to determine Pearson's correlation coefficients (*r*), which are expressed as the mean value plus or minus the standard deviation for $n = 3 \times 50$ cells. Differential interference contrast (DIC) images were employed to define the boundaries of Hep3B cells so that pixels outside of the cell boundaries could be disregarded when calculating *r*-values. VLPs were modified with an average of 60 SP94 peptides/particle and were incubated with cells for 30 min at 37 °C. Cells were counter-stained with DAPI. Scale bars = 10 μm.

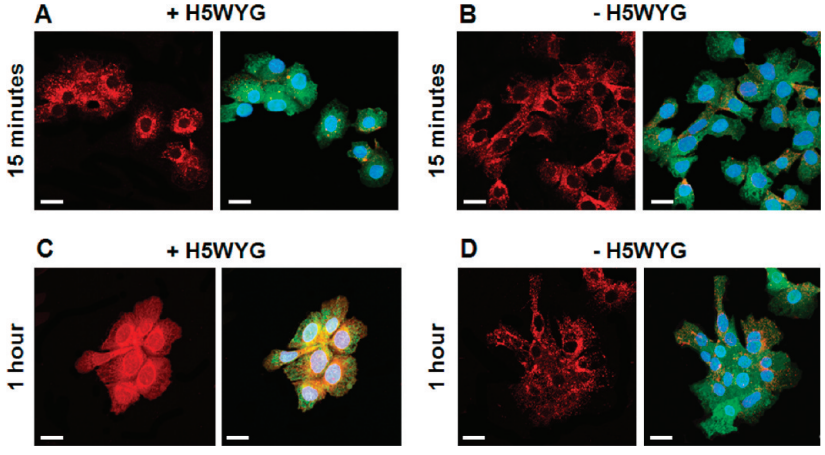

Figure 4. Upon endocytosis, VLPs comodified with the SP94 targeting peptide and the H5WYG fusogenic peptide become distributed in the cytosol of Hep3B cells, while VLPs modified with just SP94 remain localized in endosomes. (A−D) Confocal fluorescence microscopy images of Hep3B cells exposed to SP94-targeted VLPs (red) for either 15 min (A and B) or 1 h (C and D) at 37 °C. VLPs were comodified with ~60 SP94 peptides/particle and ~75 H5WYG peptides/particle in panels A and C and with ~60 SP94 peptides/particle alone in panels B and D. VLPs were labeled with Alexa Fluor 555. Cells were labeled with Hoechst 33342 and CellTracker Green CMDFA. Scale bars = 10 μm.

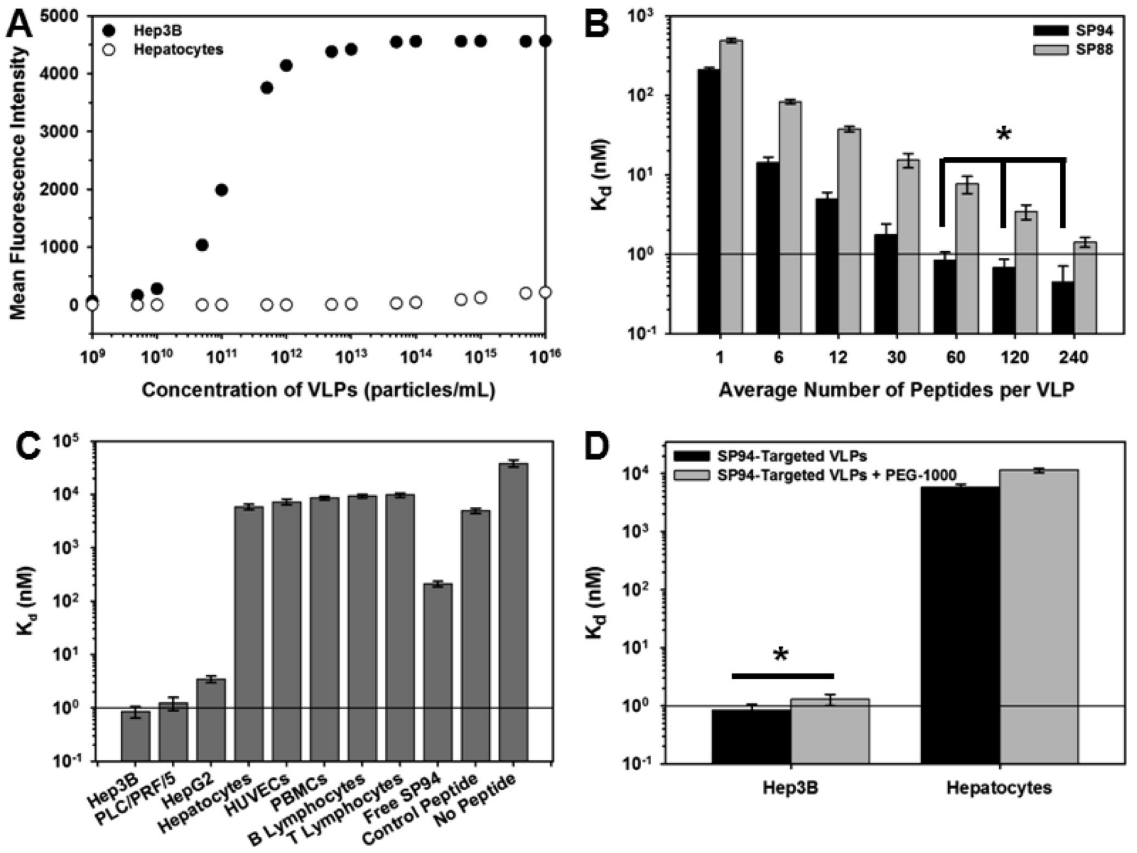

Figure 5. SP94-targeted VLPs have a high specific avidity for HCC, and the degree to which they selectively bind to HCC over hepatocytes can be modulated by peptide density and PEGylation. (A) Sample saturation binding curves for SP94-targeted VLPs (~60 peptides/particle) when exposed to Hep3B ($K_d = 5.1 \times 10^{11}$ particles/mL = 0.85 nM) or hepatocytes ($K_d = 3.5 \times 10^{15}$ particles/mL = 5.8 μM). Saturation binding curves were used to calculate dissociation constants (K_d), which are inversely related to specific avidity. (B) K_d values for VLPs modified with various densities of SP94 or SP88 targeting peptides when exposed to Hep3B. The asterisk (*) indicates values are NOT significantly different (using one-way ANOVA, $P > 0.05$ for $n = 5$). (C) K_d values for SP94-targeted VLPs (~60 peptides/particle) when exposed to HCC cells (Hep3B, PLC/PRF/5, and HepG2), hepatocytes, endothelial cells (HUVECs), and immune cells (PBMCs and B- and T-lymphocytes). The K_d values of free SP94, VLPs modified with a control peptide that has no known affinity for HCC, and unmodified VLPs (no peptide) when exposed to Hep3B are also given. (D) K_d values for VLPs, modified with the SP94 peptide alone (~60 peptides/particle) or with the SP94 peptide (~60 peptides/particle) and PEG-1000 (~145 molecules/particle) when exposed to Hep3B and hepatocytes. The asterisk (*) indicates that values are NOT significantly different (using the unpaired t test, $P > 0.05$ for $n = 5$). Cell concentrations were maintained at 1×10^6 cells/mL in all experiments. All error bars represent 95% confidence intervals (1.96 σ) for $n = 5$.

response, and mitigate nonspecific interactions with nontarget cells, all of which should increase the circulation half-life and enhance bioavailability of encapsidated cargo(s).[5] Coupling methyl-$(PEG)_{24}$-amine (MW ≈ 1000 Da; length ≈ 8.6 nm) to the MS2 capsid using EDC results in >80% modification and reduces recognition of MS2 VLPs by anti-MS2 polyclonal antibodies (data not shown). Masking a nanoparticle's surface with PEG, however, can reduce its affinity for the target cell by interfering with ligand binding.[19] Therefore, we tested the degree to which PEGylated VLPs, surface-modified with SP94 using $SM(PEG)_{24}$ (spacer arm ≈ 9.5 nm), bind to Hep3B and hepatocytes and found that PEG-1000 does not substantially affect the specific avidity of SP94-targeted VLPs for HCC but does result in a 2-fold reduction in the nonspecific binding of SP94-targeted VLPs to hepatocytes (see Figure 5D). For these reasons, VLPs used in the targeted delivery experiments described below were routinely PEGylated as detailed in the Methods section.

Delivery of a Chemotherapeutic Drug Cocktail to HCC *via* SP94-Targeted VLPs Induces Selective Cytotoxicity. Having established that the SP94 peptide promotes selective binding and internalization of VLPs by HCC, we then tested the ability of SP94-targeted VLPs to effectively deliver the chemotherapeutic drugs, doxorubicin (DOX), cisplatin, and 5-fluorouracil (5-FU), a cocktail known to be particularly effective against HCC.[20] Hep3B cells express moderate levels of P-glycoprotein (Pgp), an efflux pump that is typically upregulated by cells during acquisition of a $MDR1^+$ phenotype and that results in reduced intracellular accumulation of certain drugs, including anthracyclines like DOX.[21] To enhance the natural resistance of Hep3B to anthracyclines, we incubated parental cells in increasing concentrations of DOX for a period of 3 weeks. The concentration of

free DOX necessary to kill 50% of Hep3B with an induced MDR1$^+$ phenotype (LC_{50}) is 285.6 ± 8.2 nM, a value that can be reduced *via* inhibition of Pgp using cyclosporin A (CsA)[21] or by addition of cisplatin and 5-FU, neither of which are substrates for Pgp[20,22] (see Figure 6A). Targeted nanocarriers internalized *via* receptor-mediated endocytosis are typically able to circumvent Pgp efflux mechanisms and can, therefore, kill MDR cancer cells at lower drug concentrations.[23,24] To this end, we loaded MS2 and Qβ VLPs with an estimated 79 ± 6 molecules of DOX (per VLP). Figure 6A shows that DOX-loaded, SP94-targeted VLPs kill MDR1$^+$ Hep3B at IC_{50} values of 10−15 nM, a 20-fold improvement in the cytotoxicity of free DOX. Moreover, VLPs loaded with DOX (38 ± 4 per VLP), cisplatin (43 ± 5 per VLP), and 5-FU (111 ± 13 per VLP) kill 50% of MDR1$^+$ Hep3B at concentrations <1 nM (Figure 6A). Figure 6B compares the time-dependent (24 h and 7 days) cytotoxicity of DOX and the DOX/cisplatin/5-FU cocktail, when delivered to MDR1$^+$ Hep3B and normal hepatocytes in their free forms or encapsidated within SP94-targeted MS2 and Qβ VLPs. Free drugs are highly toxic to both Hep3B and hepatocytes, as evidenced by the near-zero viability of cells exposed to the cocktail for 24 h. In contrast, encapsidation of the drug(s) within SP94-targeted VLPs confers a high degree of specificity for HCC: nearly 100% of MDR1$^+$ Hep3B cells are dead within 7 days, while hepatocyte viability remains relatively unaffected. We attribute the 10% decrease in hepatocyte viability induced by DOX-loaded MS2 VLPs to time-dependent degradation of the capsid, which, over a period of 7 days, releases a sufficient concentration of free DOX to kill some hepatocytes. When we employed SP94-targeted VLPs of Qβ, a 28.5-nm icosahedral bacteriophage that is more stable than MS2 due to disulfide cross-linking of its capsid, MDR1$^+$ Hep3B cells were killed with similar efficacy, but long-term cytotoxicity of hepatocytes was largely mitigated (Figure 6B).

SP94-Targeted VLPs Loaded With a Cocktail of Anti-cyclin siRNAs Induce Growth Arrest and Apoptosis of HCC. The activation of certain cyclins and cyclin-dependent kinases (Cdks), including cyclin A, cyclin D1, cyclin E, and Cdk4, has been implicated in hepatocarcinogenesis.[25] Furthermore, siRNA-mediated silencing of cyclin B1 and cyclin E enhances the susceptibility of various cancer types to chemotherapeutic drugs and induces growth arrest and apoptosis of HCC.[26−28] To test the suitability of MS2 VLPs for siRNA delivery, we loaded them with a cocktail of siRNAs that silence expression of cyclin A2, cyclin B1, cyclin D1, and cyclin E1. The siRNA mixture induced assembly of intact capsids in the absence of the *pac* site (see the TEM image in Figure 1), resulting in VLPs that encapsidate an average of 84 ± 3 RNA molecules (per VLP). We additionally found that siRNA-loaded VLPs are stable for >3 months when stored in 1X PBS at 4 °C and protect encapsidated siRNA from RNase-mediated degradation (data not shown). SP94-targeted VLPs that encapsidate the siRNA cocktail induce apoptosis in >90% of Hep3B within 36 h at a siRNA concentration of 150 pM without substantially affecting the viability of hepatocytes (see Figure 7A). To determine the mechanism by which cyclin-specific siRNAs induce apoptosis of Hep3B, we also assayed for proliferation, growth arrest, and cyclin protein and mRNA concentrations. As demonstrated by Figure 7B, SP94-targeted VLPs loaded with cyclin A2, D1, and E1-specific siRNAs reduce the number of proliferating cells from ∼80% to ∼10% and increase the number of cells in G_0/G_1 from ∼25% to ∼90% within 72 h at a siRNA concentration of 150 pM; the cyclin B1-specific siRNA was omitted from this experiment since it induced G_2/M arrest and, therefore, made it difficult to discern a trend in the percentage of G_0/G_1-arrested cells *versus* time. SP94-targeted VLPs loaded with cyclin-specific siRNAs also induce a dose-dependent (Figure 7C) and time-dependent (Figure 7D) decrease in the concentrations of target proteins, presumably due to siRNA-mediated degradation of cyclin mRNAs; to confirm this hypothesis, we used real-time PCR to demonstrate that SP94-targeted VLPs loaded with the cyclin A2-specific siRNA induce a dose- and time-dependent decrease in cyclin A2 mRNA concentrations (see the red curves in Figure 7C,D, respectively). As determined from the dose−response curves shown in Figure 7C, the concentrations of siRNA necessary to silence 90% of cyclin A2, B1, D1, and E1 protein expression (IC_{90}) within 48 h when delivered to Hep3B *via* SP94-targeted VLPs are 152 ± 4.3, 164 ± 2.5, 171 ± 3.9, and 201 ± 7.8 pM, respectively. These IC_{90} values are all within 10% of the silencing efficacy achieved by delivering the same siRNAs to Hep3B using the commercially available transfection reagent, Lipofectamine RNAiMAX (see Figure 8A). Unlike the nonspecific transfection reagent, however, SP94-targeted VLPs are able to selectively silence cyclin expression in Hep3B without affecting cyclin concentrations in hepatocytes (see Figure 8B). It should be noted that the VLPs used to deliver siRNA cocktails were always comodified with SP94 and H5WYG; SP94-targeted, siRNA-loaded VLPs induce apoptosis in fewer than 15% of Hep3B cells in the absence of the H5WYG fusogenic peptide.

Ricin Toxin A-Chain Induces Specific Intoxication of HCC at Femtomolar Concentrations when Delivered by SP94-Targeted VLPs. Ricin is a potent protein toxin derived from the seeds of *Ricinis communis* and exerts its cytotoxic effect *via* catalytic inhibition of protein synthesis. Native ricin is a heterodimer composed of the catalytically active A-chain, which inactivates eukaryotic ribosomes, and the galactose-binding B-chain, which utilizes its lectin activity to promote receptor-mediated endocytosis of the toxin.[29,30] Brown *et al.* have demonstrated that MS2 VLPs can be loaded with ricin toxin A-chain (RTA), modified with transferrin (Tf), and delivered to a

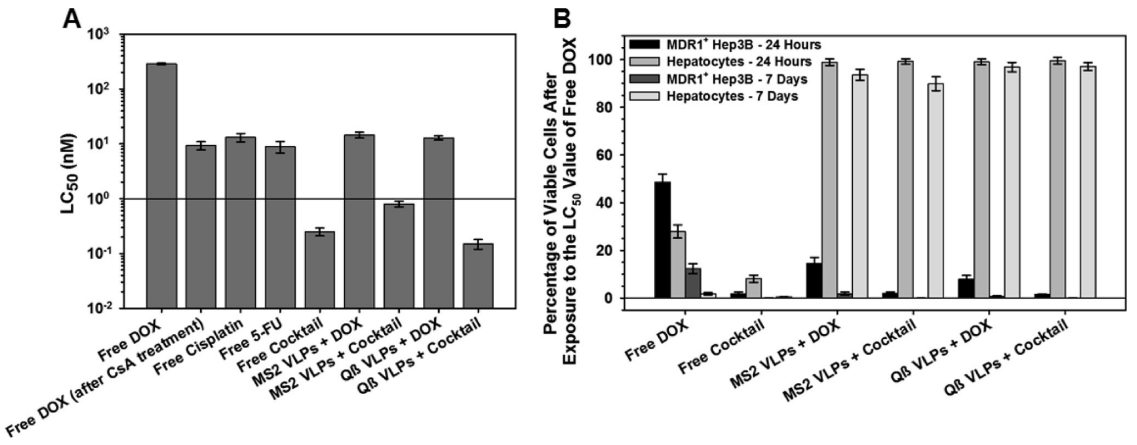

Figure 6. SP94-targeted VLPs of MS2 and structurally related bacteriophages (*e.g.*, Qβ) can deliver a sufficient concentration of chemotherapeutic agents to kill drug-resistant HCC without substantially affecting the viability of hepatocytes. (A) The concentrations of doxorubicin (DOX), cisplatin, 5-fluorouracil (5-FU), a drug cocktail (DOX, cisplatin, and 5-FU), DOX-loaded VLPs, and VLPs loaded with the drug cocktail that are necessary to kill 50% of Hep3B with an induced MDR1$^+$ phenotype (LC_{50} values) within 24 h at 37 °C. MDR1$^+$ Hep3B were exposed to cyclosporin A (CsA) to reverse Pgp-mediated resistance to DOX. (B) The percentage of MDR1$^+$ Hep3B and hepatocytes that remain viable upon continual exposure to 285 nM of free drugs or drug-loaded VLPs for either 24 h or 7 days at 37 °C; 285 nM is the LC_{50} value of free DOX when exposed to MDR1$^+$ Hep3B. MS2 and Qβ VLPs were modified with SP94 (~60 peptides/particle) and PEG-1000 (~145 molecules/particle), and cell concentrations were maintained at 1 × 10^6 cells/mL in all experiments. All error bars represent 95% confidence intervals (1.96 σ) for n = 3.

human leukemic cell line, HL-60, through interaction with the transferrin receptor.[7] In these experiments, Tf-targeted, RTA-loaded VLPs caused a > 90% reduction in HL-60 viability at a concentration of ~10 nM; in comparison, nontargeted, RTA-loaded VLPs and RTA alone killed ~60% and ~40% of cells, respectively, at the same reagent concentration. We employed a similar technique to encapsidate RTA in SP94-targeted MS2 VLPs (34 ± 8 RTA molecules per VLP, on average) and observed a dose-dependent (Figure 9A) and time-dependent (Figure 9B) induction of apoptosis in HCC, as determined by activation of caspase-3. At an RTA concentration of 100 fM, ~90% of Hep3B cells become positive for caspase-3 activation within 72 h, while hepatocyte viability is essentially unaffected by a 10^4-fold higher RTA concentration (see Figure 9A), even after continual exposure for 2 weeks (data not shown). Induction of apoptosis correlates with a dose- and time-dependent decrease in nascent protein synthesis, as demonstrated by Figure 9C,D respectively. The concentration of RTA that is necessary to reduce protein biosynthesis by 90% (IC_{90}) when delivered to Hep3B *via* SP94-targeted VLPs is 98.9 ± 3.8 fM. The IC_{90} value of RTA-loaded, SP94-targeted VLPs causes a 90% reduction in nascent protein synthesis when exposed to Hep3B for 48 h but has little effect on hepatocytes (see Figure 10A). We observe that neither nontargeted, RTA-loaded VLPs nor monomeric RTA has an effect on protein synthesis when exposed to Hep3B and hepatocytes, presumably due to the lack of cell-specific interactions needed to induce internalization (Figure 10A). Conversely, RTA-loaded MS2 VLPs, when modified with an octaarginine peptide that promotes nonspecific macropinocytosis,[31] induce rapid inhibition of protein synthesis in both Hep3B and hepatocytes (Figure 10A). It is important to note that the ability of SP94-targeted, RTA-loaded VLPs to effectively induce apoptosis of HCC depends on the presence of the H5WYG fusogenic peptide, likely because it promotes endosomal escape and prevents lysosomal degradation of RTA (see Figure 10B). Further evidence that endosomal escape of RTA-loaded VLPs is critical to induce cytotoxicity of target cells is provided by the fact that chloroquine, an agent that inhibits lysosome acidification, restores the ability of RTA-loaded VLPs modified with the SP94 peptide alone to induce activation of caspase-3 in Hep3B (Figure 10B). Using our most effective design (*i.e.*, RTA-loaded VLPs modified with ~60 SP94 peptides, ~75 H5WYG peptides, and ~145 PEG-1000 molecules), we have found that an average VLP/cell ratio of approximately 2.5 is sufficient to kill nearly the entire population of Hep3B cells.

DISCUSSION

The normal function of a virus particle is to deliver molecular cargo (normally the viral genome) to a target cell, but, thus far, comparatively little effort has been invested in repurposing VLPs for delivery of drugs and imaging agents.[32,33] The majority of such studies have focused on particles derived from Cow Pea Mosaic Virus (CPMV) or Canine Parvo Virus (CPV). CPMV has the ability to bind to and become internalized by a wide variety of mammalian cells since it naturally interacts with the cell-surface protein, vimentin.[34] In attempts to confer cell-type specificity, several other targeting ligands (*e.g.*, transferrin and folic acid) have been conjugated to the particle, with some success at directing it selectively to tumor cells. Although cell-specific binding

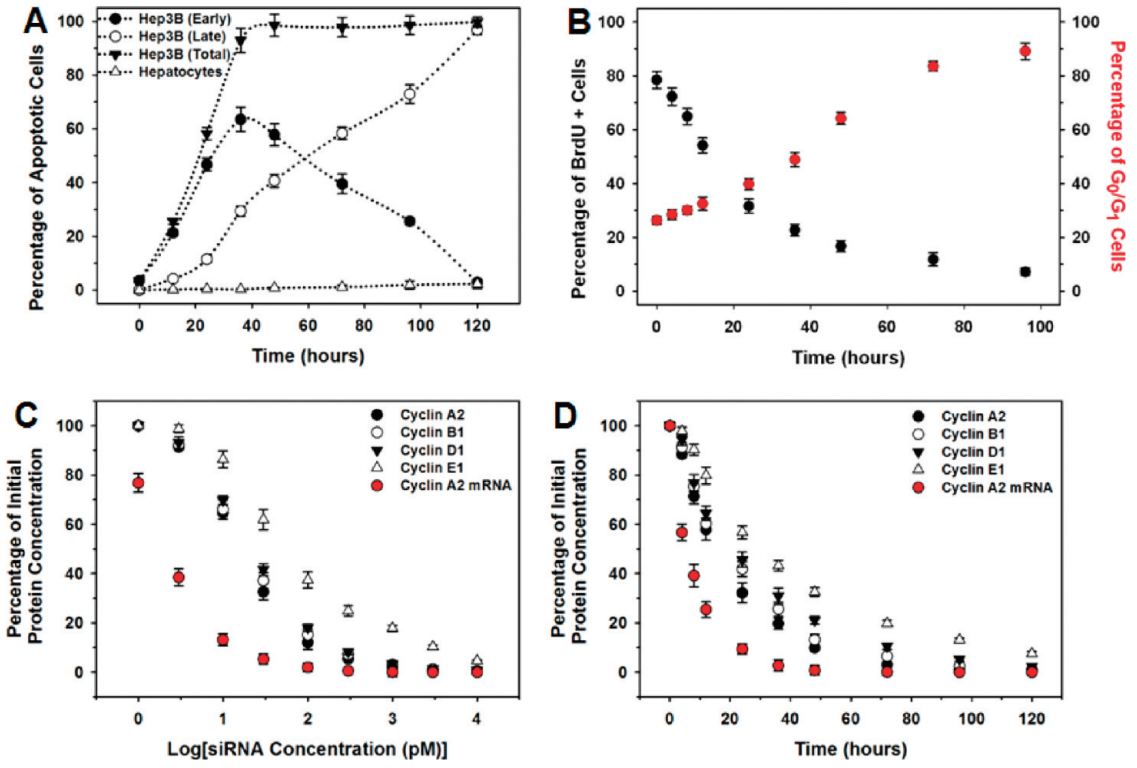

Figure 7. MS2 VLPs are naturally suited for RNA delivery, and modification of the capsid with SP94 enables targeted delivery of siRNA cocktails that silence expression of various cyclins, causing rapid growth arrest and apoptosis of HCC at picomolar concentrations. (A) The percentage of Hep3B and hepatocytes that become apoptotic upon continual exposure to SP94-targeted, siRNA-loaded VLPs for various periods of time at 37 °C. VLPs were loaded with a siRNA cocktail that silences expression of cyclin A2, B1, D1, and E1; the total siRNA concentration was maintained at 150 pM. Cells positive for Alexa Fluor 647-labeled annexin V were considered to be in the early stages of apoptosis, while cells positive for both annexin V and SYTOX Green, a cell-impermeant nucleic acid stain, were considered to be in the late stages of apoptosis. (B) The percentage of Hep3B cells that become arrested upon continual exposure to SP94-targeted, siRNA-loaded VLPs for various periods of time at 37 °C. VLPs were loaded with a siRNA cocktail that silences expression of cyclin A2, D1, and E1; the total siRNA concentration was 150 pM. The number of proliferating cells was determined by immunofluorescence-based detection of BrdU incorporation, and the number of cells arrested in G_0/G_1 was determined *via* Hoechst 33342 staining. (C) The dose-dependent decrease in cyclin A2, B1, D1, and E1 protein expression upon continual exposure of Hep3B to various concentrations of SP94-targeted, siRNA-loaded VLPs for 48 h at 37 °C. The dose-dependent decrease in cyclin A2 mRNA is included for comparison. (D) The time-dependent decrease in cyclin A2, B1, D1, and E1 protein expression upon continual exposure of Hep3B to SP94-targeted, siRNA-loaded VLPs ([siRNA] = 150 pM) at 37 °C. The time-dependent decrease in cyclin A2 mRNA is included for comparison. For panels C and D, VLPs were loaded with a single type of siRNA. Cyclin protein concentrations were determined *via* immunofluorescence, and cyclin A2 mRNA concentrations were determined by real-time PCR. VLPs were modified with SP94 (~60 peptides/particle), H5WYG (~75 peptides/particle), and PEG-1000 (~145 molecules/particle) in all experiments. All error bars represent 95% confidence intervals (1.96 σ) for $n = 3$.

has been demonstrated, we are unaware of attempts to utilize CPMV-based particles for drug delivery. Fortuitously, CPV naturally uses the transferrin receptor for cell entry during infection, and the overexpression of transferrin receptor on many tumor cell types makes the particle an attractive candidate for delivery applications. Although fluorescently labeled particles show selective binding and entry into tumor cells, CPV has not yet been utilized specifically for drug delivery.[35]

A few previous efforts to use MS2 VLPs for both drug delivery and imaging purposes have been reported, and the results have been encouraging. Wu *et al.*, for example, reported the delivery of ricin toxin A-chain (RTA) to leukemic HL-60 cells using VLPs decorated with intact transferrin protein,[7] thus taking advantage of transferrin receptor overexpression to selectively target tumor cells. These particles killed ~75% of HL-60 cells at a RTA concentration of ~1 nM, an approximate 10-fold improvement over RTA alone, which, for some reason, exhibited an unexpected level of toxicity. The same group showed that antisense DNA oligonucleotides designed to interfere with p120 expression (an essential nucleolar protein overexpressed in tumors) can be delivered to HL-60 cells, again in a transferrin-dependent fashion.[8] However, the required DNA concentration was relatively high ($LC_{50} \approx 100$ nM) and only about 100-fold lower than the naked oligonucleotide added directly to the culture medium.

Our results represent a significant improvement. For example, when delivered by our particles, ricin toxin A-chain causes 90% of Hep3B cells to apoptose within 72 h at a RTA concentration of only ~100 fM. Moreover, the specificity for HCC cells is remarkable; normal hepatocytes (and a variety of other cell types) are not

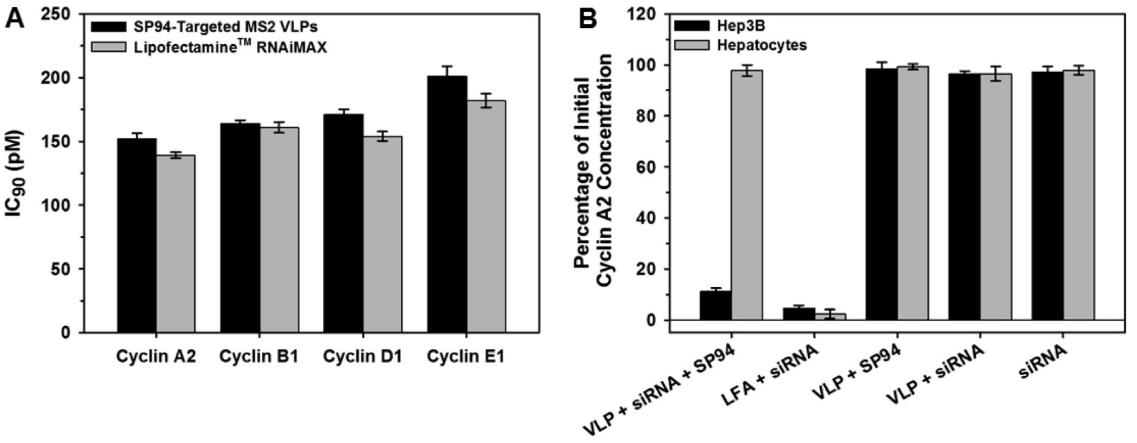

Figure 8. SP94-targeted VLPs loaded with cyclin-specific siRNAs selectively transfect HCC with efficiencies similar to that of commercially available transfection reagents. (A) The concentrations of siRNA necessary to silence 90% of cyclin A2, B1, D1, or E1 protein expression (IC_{90}) in Hep3B when delivered *via* SP94-targeted VLPs or Lipofectamine RNAiMAX (LFA). (B) The percentage of initial cyclin A2 protein expression that remains upon exposure of Hep3B and hepatocytes to cyclin A2-specific siRNA using SP94-targeted VLPs and LFA, a nonspecific transfection reagent, as delivery vehicles. Empty SP94-targeted VLPs, nontargeted, siRNA-loaded VLPs, and siRNA alone were used as controls. VLPs were modified with H5WYG (~75 peptides/particle) and PEG-1000 (~145 molecules/particle) in all experiments and with SP94 (~60 peptides/particle) when indicated. All error bars represent 95% confidence intervals (1.96 σ) for $n = 3$.

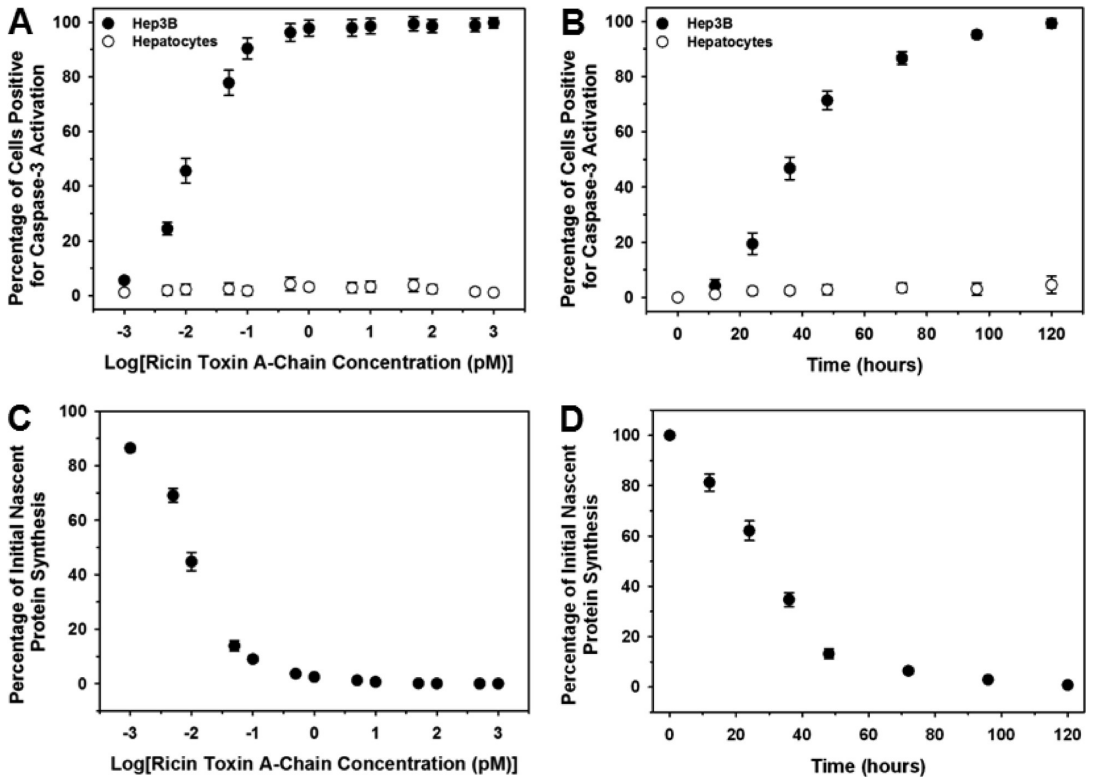

Figure 9. SP94-targeted VLPs that encapsidate ricin toxin A-chain induce apoptosis of HCC at femtomolar concentrations without affecting the viability of hepatocytes. (A) The percentage of Hep3B and hepatocytes that become positive for caspase-3 activation when continually exposed to various concentrations of SP94-targeted, ricin toxin A-chain (RTA)-loaded VLPs for 48 h at 37 °C. (B) The time-dependent activation of caspase-3 in Hep3B and hepatocytes upon exposure to SP94-targeted, RTA-loaded VLPs ([RTA] = 100 fM) at 37 °C. Caspase-3 activation was quantified using a FITC-labeled derivative of the caspase-3 inhibitor, DEVD-FMK. The dose- (C) and time- (D) dependent decrease in nascent protein synthesis that was observed upon continual exposure of Hep3B to SP94-targeted, RTA-loaded VLPs at 37 °C. Cells were exposed to various concentrations of VLPs for 48 h in panel C and to a fixed concentration of VLPs ([RTA] = 100 fM) for various periods of time in panel D. Nascent protein synthesis was quantified using an Alexa Fluor 488-labeled derivative of methionine. VLPs were modified with SP94 (~60 peptides/particle), H5WYG (~75 peptides/particle), and PEG-1000 (~145 molecules/particle) in all experiments. All error bars represent 95% confidence intervals (1.96 σ) for $n = 3$.

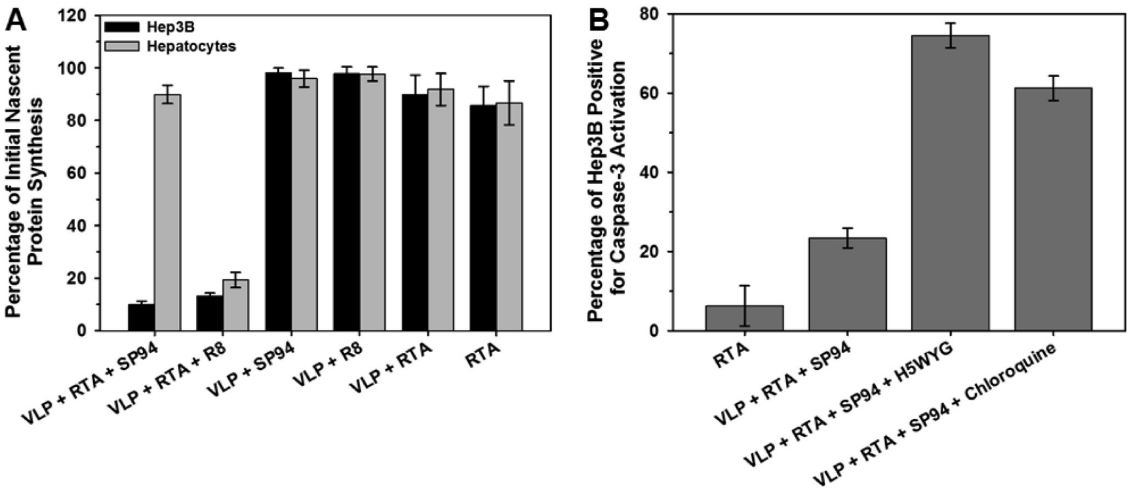

Figure 10. Codisplay of SP94 and H5WYG enables RTA-loaded VLPs to become selectively internalized by HCC and to release their cargo into the cytosol before lysosomal conditions destroy the toxin's catalytic activity. (A) The percentage of nascent protein synthesis that remains upon exposure of Hep3B and hepatocytes to RTA-loaded VLPs modified with either the SP94 peptide or with a peptide that promotes nonspecific macropinocytosis (R8). Empty SP94-modified VLPs, empty R8-modified VLPs, nontargeted VLPs loaded with RTA, and RTA alone were employed as controls. (B) The percentage of Hep3B that become positive for caspase-3 activation when exposed to RTA-loaded VLPs modified with SP94 alone or with a combination of SP94 and H5WYG. Hep3B cells were treated with chloroquine to inhibit lysosomal acidification. Cells were exposed to 100 fM of RTA for 48 h at 37 °C in all experiments. VLPs were modified with PEG-1000 (~145 molecules/particle), as well as an average of ~60 SP94 peptides, ~80 R8 peptides, and/or ~75 H5WYG peptides. All error bars represent 95% confidence intervals (1.96 σ) for $n = 3$.

detectably affected at these concentrations. Our siRNA delivery results are similarly dramatic. SP94-targeted VLPs that deliver anti-cyclin siRNAs at a concentration of 150 pM induce apoptosis in virtually 100% of Hep3B cells within 48 h without affecting the viability of normal hepatocytes. We attribute the relative efficiency of our VLPs to several factors: (i) Multivalency of the targeting peptide. Our particles can display up to 240 targeting peptides per VLP, but as few as 60 peptides are sufficient to maximize avidity and promote cell-specific internalization. The importance of multivalency has been previously demonstrated using dendrimers targeted to the folate receptor; in these studies, multivalent presentation of folic acid dramatically enhanced targeting efficacy.[36] (ii) Presence of a fusogenic peptide. We find that the potency of particles containing a protein or nucleic acid cargo (*i.e.*, ricin toxin A-chain or siRNA) is greatly enhanced by the presence of a fusogenic peptide, presumably because it promotes endosomal escape of these molecules before they can be degraded in lysosomes. (iii) PEGylation. Nanocarriers of diverse types benefit from modification with PEG.[5,19] Our particles are more stable and show less nonspecific binding activity when PEGylated. (iv) Receptor identity and ligand specificity. Although the receptor recognized by SP94 has not yet been identified, it is apparently present in high densities on HCC and mediates efficient entry by endocytosis. Moreover, it seems to be present specifically on HCC, and its absence from the other cell types we tested surely contributes to the high specificity we observe. (v). Choice of drug. Ricin toxin A-chain and anti-cyclin siRNAs are potent inducers of apoptosis. When combined with an efficient and highly specific delivery vehicle, they selectively kill target cells at sub-nanomolar concentrations.

CONCLUSIONS

MS2 VLPs can be readily adapted for specific delivery of a variety of molecular cargos to diverse cell types. Because of their natural ability to encapsidate nucleic acids, they are especially well-suited for delivering RNA- and DNA-based drugs, but they can also encapsulate diverse, non-nucleic acid cargos (*e.g.*, quantum dots, chemotherapy drugs, and protein toxins) when the cargo molecules are linked to the MS2 *pac* site. In the experiments described here, we decorated MS2 VLPs with SP94, an HCC-specific peptide, but other targeting strategies are possible. Indeed, prior work reported the use of transferrin,[7,8] of a DNA aptamer that binds to a tyrosine kinase receptor,[6] and of folic acid for this purpose.[37] The MS2 VLP platform has a special advantage when peptides are used for targeting, however. We previously showed that peptides can be displayed on the VLP surface by genetic fusion to coat protein and that these VLPs encapsidate the mRNA that encodes the fusion protein.[2] On this basis, we created a system for VLP-based peptide display analogous to conventional filamentous phage display, which allows for affinity selection of arbitrary binding activities from complex random sequence peptide libraries.[13] Selected sequences are then recovered by reverse transcription and polymerase chain reaction and recloned for synthesis of the selected VLPs in

bacteria. The existence of this affinity selection capability means that a single particle can serve both for identification of cell-specific targeting ligands and as a drug delivery vehicle.

MATERIALS AND METHODS

Materials. Antibodies against LAMP-1 (rabbit pAb), Rab11a (mouse mAb), cyclin A2 (mouse mAb), cyclin B1 (mouse mAb), cyclin D1 (mouse mAb), and cyclin E1 (mouse mAb) were purchased from Abcam, Inc. (Cambridge, MA). *Silencer* select siRNAs (siRNA IDs for cyclin A2, B1, D1, and E1 are s2513, s2515, s229, and s2526, respectively) and the TaqMan Fast Cells-to-CT Kit were purchased from Applied Biosystems by Life Technologies Corporation (Carlsbad, CA). Human Hep3B (HB-8064), human hepatocytes (CRL-11233), human peripheral blood mononuclear cells (CRL-9855), human umbilical cord vein endothelial cells (CRL-2873), T lymphocytes (CRL-8293), B lymphocytes (CCL-156), Eagle's Minimum Essential Medium (EMEM), Dulbecco's Modified Eagle's Medium (DMEM), Iscove's Modified Dulbecco's Medium (IMDM), RPMI 1640 medium, fetal bovine serum (FBS), and 1X trypsin-EDTA solution (0.25% trypsin with 0.53 mM EDTA) were purchased from American Type Culture Collection (ATCC; Manassas, Virginia). CaspGLOW Fluorescein Active Caspase-3 Staining Kit (485/535) was purchased from BioVision, Inc. (Mountain View, CA). Reactive forms of the *pac* site were synthesized by Integrated DNA Technologies (Coralville, IA). Hoechst 33342 (350/461), 4,6-diamidino-2-phenylindole (DAPI, 356/451), CellTracker Violet BMQC (415/516), CellTracker Green CMFDA (492/517), Ulysis Alexa Fluor 488 Nucleic Acid Labeling Kit (495/519), Alexa Fluor 488 Antibody Labeling Kit (495/519), Alexa Fluor 488 conjugate of annexin V (495/519), Alexa Fluor 488-labeled mouse monoclonal antibody to BrdU (clone MoBU-1) (494/519), Alexa Fluor 488 goat anti-mouse IgG (H+L) (495/519), Alexa Fluor 488 goat anti-rabbit IgG (H+L) (495/519), Click-iT AHA Alexa Fluor 488 Protein Synthesis HCS Assay (495/519), SYTOX Green nucleic acid stain (504/523), Alexa Fluor 532 carboxylic acid succinimidyl ester (532/554), Alexa Fluor 555 C_2 maleimide (555/565), Alexa Fluor 555 hydrazide (555/565), Alexa Fluor 555 carboxylic acid succinimidyl ester (555/565), Qdot 585 ITK amino(PEG) (300/585), pHrodo succinimidyl ester (560/586), propidium iodide (535/617), Ulysis Alexa Fluor 647 Nucleic Acid Labeling Kit (650/668), Alexa Fluor 647 conjugate of annexin V (650/668), Alexa Fluor 647 goat anti-mouse IgG (H+L) (650/668), *SlowFade* Gold antifade reagent (with and without DAPI), Image-iT FX signal enhancer, Lipofectamine RNAiMAX, 1X Dulbecco's phosphate-buffered saline (D-PBS), bovine albumin fraction V solution (BSA, 7.5%), and transferrin were purchased from Invitrogen Life Sciences (Carlsbad, CA). BEGM Bullet Kits were purchased from Lonza Group Limited (Clonetics; Walkersville, MD). Amicon Ultra-4 Centrifugal Filter Units (3 kDa, 50 kDa, and 100 kDa MWCO) were purchased from Millipore (Billerica, MA). All peptides were synthesized by New England Peptide (Gardner, MA). Sulfosuccinimidyl 6-(3′-[2-pyridyldithio]-propionamido)hexanoate (Sulfo-LC-SPDP), succinimidyl-[(*N*-maleimidopropionamido)-tetracosaethyleneglycol] ester (SM(PEG)$_{24}$), 1-ethyl-3-[3-dimethylaminopropyl]carbodiimide hydrochloride (EDC), methyl-(ethyleneglycol)-24amine (MA(PEG)$_{24}$), Slide-A-Lyzer MINI dialysis units (20 kDa MWCO), and Slide-A-Lyzer G2 dialysis cassettes (3.5 kDa MWCO) were purchased from Pierce Protein Research Products (Thermo Fisher Scientific LSR; Rockford, IL). Ultra pure, EM-grade formaldehyde (16%, methanol-free) was purchased from Polysciences, Inc. (Warrington, PA). Sephadex G-75, Triton X-100 hexadecane (≥99%), cyclosporin A from *Tolypocladium inflatum* (CsA, > 95%), 5-bromo-2′-deoxyuridine (BrdU, ≥ 99%), chloroquine diphosphate salt (≥98%), human epidermal growth factor, L-α-phosphatidylethanolamine, thymidine (≥99%), hypoxanthine (≥99%), bovine fibronectin, bovine collagen type I, gelatin, soybean trypsin inhibitor (≥98%), DMEM without phenol red, goat serum, doxorubicin hydrochloride (≥98%), 5-fluorouracil (≥99%), *cis*-diammineplatinum(II) dichloride (cisplatin, ≥ 99.9%), and deglycosylated A-chain from *Ricinus communis* were purchased from Sigma-Aldrich (St. Louis, MO). Spectra/Por dialysis tubing (15 kDa MWCO) was purchased from Spectrum Laboratories, Inc. (Rancho Dominguez, CA).

Cell Culture. Hep3B, HepG2, PLC/PRF/5, hepatocytes, PBMCs, T-lymphocytes, and B-lymphocytes were obtained from ATCC and grown per manufacturer's instructions. Briefly, Hep3B, HepG2, and PLC/PRF/5 were maintained in EMEM with 10% FBS. Hepatocytes were grown in flasks coated with BSA, fibronectin, and bovine collagen type I; the culture medium used was BEGM (gentamycin, amphotericin, and epinephrine were discarded from the BEGM Bullet kit) with 5 ng/mL epidermal growth factor, 70 ng/mL phosphatidylethanolamine, and 10% FBS. HUVECs were grown in DMEM with 20% FBS; gelatin-coated flasks were used to promote adhesion. PBMCs, T lymphocytes, and B lymphocytes were maintained in suspension flasks (Greiner Bio-One; Monroe, NC). PBMCs were grown in IMDM supplemented with 0.02 mM thymidine, 0.1 mM hypoxanthine, 0.05 mM 2-mercaptoethanol, and 10% FBS. T and B lymphocytes were grown in IMDM with 20% FBS and RPMI 1640 medium with 20% FBS, respectively. All cells were maintained at 37 °C in a humidified atmosphere (air supplemented with 5% CO_2). Adherent cells were passaged with 0.05% trypsin at a subcultivation ratio of 1:3, while non-adherent cells were seeded at a density of ~1×10^5 cells/mL and maintained at $(1-5) \times 10^6$ cells/mL.

Disassembly of MS2 and Qβ Bacteriophages. MS2 and Qβ bacteriophages were produced by infecting *E. coli* A/λ using well-established procedures[38] and purified by sedimentation to equilibrium in CsCl density gradients. To harvest coat protein dimers for reassembly reactions, MS2 phage (10 mg/mL) was diluted 1:3 in cold glacial acetic acid, incubated for 2 h at 4 °C, and centrifuged briefly to pellet precipitated RNA and maturase. Qβ phage (10 mg/mL) was incubated in 50 mM Trizma hydrochloride with 6 M urea and 10 mM dithiothreitol (pH 8.5) for 1 h at 4 °C and centrifuged briefly to remove precipitated RNA. The resulting protein was dialyzed against 10 mM acetic acid with 50 mM NaCl (~pH 4) using regenerated cellulose tubing (15 kDa MWCO); buffer (1.5 L) was changed twice in 12-h intervals. Dialyzed protein was then applied to a 0.9 × 45 cm Sephadex G-75 column and eluted using 10 mM acetic acid with 50 mM NaCl (~pH 4); ~1 mL fractions were collected and assayed for protein content *via* agarose gel electrophoresis; gels (1%) were stained with Coomassie Brilliant Blue R-250 to enable visualization of protein. Fractions that contained coat protein dimers (~28 kDa) were pooled, concentrated using a centrifugal filter unit (10 kDa MWCO), resuspended in 10 mM acetic acid with 50 mM NaCl (~pH 4), and stored at 4 °C for no more than 2 weeks. The concentrations of coat protein dimers were measured using UV spectroscopy immediately before their use in reassembly reactions.

Modification of Various Therapeutic and Diagnostic Agents with the *pac* Site. Various reactive forms of the *pac* site were synthesized, including those with (1) a 3′ sulfhydryl moiety, (2) a 3′ amine moiety, or (3) three internal 5-fluorouridines and a 5′ thiol group. All *pac* site derivatives contained a uracil spacer (3−9 nucleotides in length) between the wild-type sequence and the reactive group. To prepare quantum dot-*pac* site conjugates, Qdot 585 ITK amino(PEG), a CdSe/ZnS (core/shell) quantum dot passivated with amine-terminated PEG, was diluted to 1 μM with 1X PBS and incubated with a 10-fold molar excess of Sulfo-LC-SPDP, a thiol-cleavable, amine-to-sulfhydryl cross-linker, for 2 h at room temperature; excess cross-linker was removed *via* centrifugal filtration (50 kDa MWCO). SPDP-activated quantum dots were then incubated with a 10-fold molar excess of the sulfhydryl-modified *pac* site for 12 h at 4 °C. Unreacted RNA was removed using a centrifugal filter device (50 kDa MWCO), and quantum dot-*pac* site conjugates were resuspended in 50 mM

Tris-HCl (pH 8.5) at a quantum dot concentration of 10 μM. The average number of *pac* sites per quantum dot was determined by exposing 5 μL of the conjugate to 10 mM DTT for 1 h at room temperature, dialyzing the resulting solution to remove liberated *pac* site molecules (Slide-A-Lyzer MINI Dialysis Units, 20 kDa MWCO), and measuring the absorbance of the solution at 260-nm (A_{260}) before and after RNA removal.

To prepare doxorubicin-*pac* site conjugates, the sulfhydryl-modified *pac* site was diluted to 5 μM with 1X PBS and incubated with a 10-fold molar excess of Sulfo-LC-SPDP and a 5-fold molar excess of doxorubicin (DOX), which contains a primary amine group, for 2 h at room temperature and then 12 h at 4 °C. The reaction mixture was dialyzed (Slide-A-Lyzer Cassette, 3.5 kDa MWCO) against 50 mM Tris-HCl (pH 8.5) to remove unreacted cross-linker and drug; conjugates were concentrated *via* centrifugal filtration (3 kDa MWCO) and resuspended in 50 mM Tris-HCl (pH 8.5) at a RNA concentration of 50 μM. The degree of labeling (*i.e.*, the number of DOX molecules per *pac* site) was determined using the following equation:

$$\text{degree of labeling} = \frac{A_{484} \times (\text{molecular weight of } pac \text{ site})}{[pac \text{ site}(\text{mg/mL})] \times \varepsilon_{DOX}}$$

where A_{484} is the absorbance of the DOX-pac site conjugate at 484 nm (λ_{max} for DOX) and $\varepsilon_{DOX} = 10800\ cm^{-1}\ M^{-1}$.

To prepare *pac* sites modified with a combination of DOX, cisplatin, and 5-fluorouracil (5-FU), the *pac* site with three internal 5-fluorouridines and a 5′ thiol group was first reduced *via* exposure to 10 mM DTT for 2 h at room temperature and desalted using a polyacrylamide desalting column (1.8 kDa MWCO). Five μM of the reduced *pac* site was incubated for 2 h at room temperature and then 12 h at 4 °C with a 10-fold molar excess of Sulfo-LC-SPDP and a 5-fold molar excess of DOX and cisplatin, both of which contain primary amine groups. Unreacted cross-linker and drugs were removed as described above. Conjugates were concentrated *via* centrifugal filtration (3 kDa MWCO) and resuspended in 50 mM Tris-HCl (pH 8.5) at a RNA concentration of 50 μM. The DOX/*pac* site ratio was determined as described above, and the cisplatin/*pac* site ratio was measured according to the technique described by Anilanmert *et al.*[39]

Ricin toxin A-chain-*pac* site conjugates were synthesized as described previously[7] with minor modifications. Briefly, the amine-modified *pac* site (5 μM in 1X PBS) was incubated with a 10-fold molar excess of Sulfo-LC-SPDP for 2 h at room temperature and then 12 h at 4 °C; unreacted cross-linker was removed *via* dialysis (Slide-A-Lyzer Cassette, 3.5 kDa MWCO) against 1X PBS. A 1 mg portion of deglycosylated ricin toxin A-chain (RTA) was reduced by exposure to 10 mM DTT for 2 h at room temperature and desalted using a polyacrylamide desalting column (6 kDa MWCO). Reduced RTA (1 μM in 1X PBS), which contains a free cysteine residue, was immediately combined with a 5-fold molar excess of the SPDP-activated *pac* site, flushed with nitrogen gas, and incubated at room temperature for 4 h and then at 4 °C for 24 h. Unreacted RNA was removed *via* centrifugal-driven filtration (10 kDa MWCO), conjugates were resuspended in 50 mM Tris-HCl (pH 8.5) at a RTA concentration of 10 μM, and the cross-linking efficiency was determined using UV spectroscopy and SDS-PAGE. A 10 μg portion of the RTA-*pac* site conjugate was fluorescently labeled per manufacturer's instructions using the Ulysis Alexa Fluor 488 Nucleic Acid Labeling Kit. It is important to note that Sulfo-LC-SPDP is a thiol-cleavable cross-linker, which enables liberation of cargo from the *pac* site upon exposure to the reducing intracellular environment.

MS2 VLPs that encapsidate cyclin-specific siRNAs were synthesized as described below; linkage of siRNA to the *pac* site was unnecessary, however, due to the ability of MS2 coat protein to nonspecifically package RNA *in vitro*. A 10 μg portion of cyclin A2-specific siRNA was fluorescently labeled per manufacturer's instructions using the Ulysis Alexa Fluor 647 Nucleic Acid Labeling Kit.

Encapsidation of Various Cargos within MS2 and Qβ VLPs. Coat protein dimers were concentrated to 1 mM in 10 mM acetic acid with 50 mM NaCl (~pH 4), while siRNA and *pac* site-modified cargos were diluted to 10 μM (total RNA concentration) with 50 mM Tris-HCl (pH 8.5). Dimerized coat protein (1 nmol) was then incubated with 1000, 500, 250, 125, or 62.5 pmol of RNA for 1 h at room temperature, and reassembly efficiency was assessed using agarose gel electrophoresis as described previously.[40] On the basis of these results, a 4-fold molar excess of dimerized coat protein was used in most reassembly reactions. For example, 100 μL of *pac* site-modified quantum dots (10 μM of RNA, which corresponds to ~0.125 μM of quantum dots) was combined with 40 μL of MS2 dimers (1 mM). Reassembly reaction mixtures were applied to a 0.9 × 45 cm Sephadex G-75 column in order to remove excess coat protein and unencapsidated cargos. VLPs were eluted using 50 mM Tris-HCl (pH 8.5). 1 mL fractions were collected and assayed for protein content *via* agarose gel electrophoresis; gels (1%) were stained with Coomassie Brilliant Blue R-250 to enable visualization of protein. Fractions that contained reassembled VLPs were pooled and concentrated using a centrifugal filter unit (100 kDa MWCO); VLPs were extensively washed (6−10 times) and resuspended in 1X PBS.

To determine the average number of cargo molecules per VLP, 10 μL of purified, concentrated VLPs were incubated in 50 mM Tris-HCl (pH 8.5) with 6 M urea and 10 mM DTT for 1 h at room temperature; the resulting samples were subjected to SDS-PAGE to determine coat protein and RTA concentrations, UV spectroscopy (A_{260}) to determine siRNA and *pac* site concentrations, and fluorimetry to determine quantum dot and DOX concentrations. Reassembled VLPs were further characterized by electron microscopy (according to the procedure described by Kovacs *et al.*[5]) to determine the fraction of intact capsids.

Modification of VLP Capsids with Peptides and PEG. All peptides were synthesized with a C-terminal cysteine residue, separated from the reported sequence by a $(Gly)_2$ spacer, and conjugated to surface lysine residues present in the MS2 (or Qβ) capsid using the heterobifunctional cross-linker, $SM(PEG)_{24}$, which is reactive toward amine and sulfhydryl groups and contains a PEG spacer arm 9.5-nm in length. Cross-linkers with PEG spacers were used to reduce the potential for any steric hindrance of ligand binding and to enable subsequent PEGylation of the MS2 surface, which reduces nonspecific interactions and prevents recognition of MS2 VLPs by anti-MS2 antibodies (see below for more details). VLPs were incubated with a 10-fold molar excess of $SM(PEG)_{24}$ for 2 h at room temperature, and excess cross-linker was removed using a centrifugal filtration device (100 kDa MWCO). Activated capsids were immediately incubated with various concentrations of peptides (0.1 to 10-fold molar excess) for either 1 h at room temperature or 12 h at 4 °C; unreacted peptides were removed *via* centrifugal filtration. Average peptide density was determined using SDS-PAGE. ImageJ Image Processing and Analysis Software was utilized to compare band intensities relative to a standard concentration curve. The targeting peptide employed in the majority of studies was SP94 (H_2N-SFSIIHTPILPL-COOH[14]), an HCC-specific peptide previously identified by phage display. Some experiments utilized a second targeting peptide (SP88, H_2N-ELMNPLLPFIQP-COOH[14]), which has a slightly lower inherent affinity for HCC than SP94. Control experiments were conducted using VLPs modified with an irrelevant peptide (H_2N-FPWFPLPSPYGN-COOH[14]) that does not bind to HCC. Endosomal escape of internalized VLPs was promoted by a histidine-rich fusogenic peptide (H5WYG, H_2N-GLFHAIAHFIHGGWHGLIHGWYG-COOH[15]), and nonspecific macropinocytosis of RTA-loaded VLPs was stimulated using a peptide composed of eight arginine residues (R8[31]).

VLPs were PEGylated *via* incubation with a 5-fold molar excess of EDC-activated $MA(PEG)_{24}$ for 12 h at 4 °C; capsids were purified *via* centrifugal filtration (100 kDa MWCO), and the extent of PEGylation was determined using SDS-PAGE, as described previously.[5] The degree to which polyclonal anti-MS2 antibodies bind to PEGylated and non-PEGylated VLPs was determined using a sandwich ELISA assay, as described previously;[5] an Alexa Fluor 488-labeled goat anti-mouse IgG secondary antibody was employed in place of the HRP-modified primary antibody used by Kovacs *et al.*

VLPs were fluorescently labeled, per manufacturer's instructions, with Alexa Fluor 555 hydrazide (in conjunction with EDC)

for the experiments depicted in Figures 2B,C, 3, 4, and 5A–C, with Alexa Fluor 555 carboxylic acid succinimidyl ester for the experiments depicted in Figure 5D, and with Alexa Fluor 532 carboxylic acid succinimidyl ester for the experiment depicted in Figure 2A. To determine the average number of SP94-targeted VLPs internalized by Hep3B and hepatocytes, the capsid was labeled with Alexa Fluor 488 hydrazide (in conjunction with EDC) and pHrodo succinimidyl ester per manufacturer's instructions.

Determination of Dissociation Constants. Adherent and nonadherent cells were grown in suspension flasks to 70–80% confluence or $(2–4) \times 10^6$ cells/mL, respectively. Adherent cells were harvested *via* gentle shaking in 5 mM EDTA (diluted in D-PBS) for 30 min at 37 °C. Cells were counted (Cellometer automated cell counter; Nexcelom Biosciences; Lawrence, MA), and 1×10^6 cells/mL were placed in siliconized tubes, centrifuged at 4000 rpm for 2 min, washed twice with 1X D-PBS, and resuspended in complete growth medium. Increasing concentrations of monovalent peptides (labeled with Alexa Fluor 555 C_2 maleimide) or VLPs (labeled with Alexa Fluor 555 hydrazide or Alexa Fluor 555 carboxylic acid succinimidyl ester) were incubated with 1×10^6 cells/mL for 1 h at 4 °C under gentle agitation. One hour is a sufficient period of time for the number of surface-bound particles to reach equilibrium; SP94 and SP88-targeted VLPs exhibit saturable binding (see Figure 5A). Cells were washed four times with 1X D-PBS, and resuspended in 1 mL of serum-free DMEM without phenol red. Cell samples were immediately analyzed with a FACSCalibur flow cytometer (Becton Dickinson; Franklin Lakes, NJ) equipped with BD CellQuest software, version 5.2.1. Data were acquired with the FSC channel in linear mode and all other channels in log mode. Events were triggered based upon forward light scatter, and a gate was placed on the forward scatter-side scatter plot that excluded cellular debris. Samples were excited using the 488-nm laser source, and emission intensity was collected in the FL-2 channel (585/42 filter/bandpass). Mean fluorescence intensity (MFI) was determined using FlowJo Software, version 6.4 (Tree Star, Inc.; Ashland, OR). Cells saturated with SP94-targeted VLPs, monovalent SP94, *etc.* were incubated with ~1 μM of unlabeled SP94 (*i.e.*, the saturating concentration of the monovalent peptide) for 1 h at 4 °C, and resulting MFIs were remeasured to determine nonspecific binding. Data points that required VLP concentrations of $\geq 1 \times 10^{14}$ particles/mL were collected in 384-well plates using 10–50 μL volumes. Fluorescence emission intensities were determined using a SpectraMax M2e microplate reader (Molecular Devices, Inc.; Sunnyvale, CA); settings were adjusted so that the MFIs of samples exposed to lower VLP concentrations were similar to MFIs collected using flow cytometry. GraphPad Prism (GraphPad Software, Inc.; La Jolla, CA) was used to generate saturation binding curves (ligand or VLP concentration *versus* MFI), subtract the contribution of nonspecific binding (*e.g.*, binding of SP94-targeted VLPs in the presence of free SP94) from total binding (*e.g.*, binding of SP94-targeted VLPs), and calculate K_d values. GraphPad InStat (GraphPad Software, Inc.; La Jolla, CA) was used to perform the statistical analyses (one-way analysis of variance (ANOVA) and unpaired *t* test) summarized in the Figure 5 caption. Plots were generated using Sigma Plot, version 11.0 (Systat Software, Inc.; San Jose, CA).

Determination of the Average Numbers of Internalized VLPs. The average number of SP94-targeted VLPs internalized by each Hep3B or hepatocyte cell was determined using the following procedure. VLPs were labeled, per manufacturer's instructions, with Alexa Fluor 488 hydrazide (in conjunction with EDC) and pHrodo succinimidyl ester after conjugation of the SP94 peptide; pHrodo SE becomes more fluorescent upon acidification of its environment, that is, during endocytosis. 1×10^6 cells/mL were exposed to increasing concentrations of particles (1×10^6 to 1×10^{10}) for 1 h at 4 °C, washed, and resuspended in cold DMEM without phenol red. Samples were analyzed using a FACSCalibur flow cytometer and gated as described above. Alexa Fluor 488 was excited with the 488-nm laser, and emission intensity was collected in the FL1 channel (530/30 filter/bandpass). Mean fluorescence intensity (MFI) was determined using FlowJo Software, and MFI *versus* particle concentration data were transformed into Scatchard plots using GraphPad Prism. The average numbers of particles that bind to each Hep3B or hepatocyte cell under saturating conditions were calculated from B_{max} values. Samples were then incubated at 37 °C for 1 h to enable endocytosis of surface-bound particles, and the MFIs of Alexa Fluor 488 and pHrodo SE were measured and plotted against particle concentration; for pHrodo SE, the 488-nm laser was used as the excitation source, and emission intensity was collected in the FL2 channel. B_{max} values were determined from Scatchard plots and used to calculate the average number of SP94-targeted VLPs endocytosed by each Hep3B or hepatocyte cell within an hour. Alexa Fluor 488 was used to determine the total number of particles associated with each cell, while pHrodo was used to determine the number of particles localized within acidic compartments.

Preparation and Analysis of Confocal Fluorescence Microscopy Samples. 1×10^4 to 1×10^6 cells/mL were seeded on sterile coverslips (25-mm, no. 1.5) coated with 0.01% poly-L-lysine (150–300 kDa), and these were allowed to adhere for 4–24 h at 37 °C. Cells were incubated with a 5000-fold excess of SP94-targeted VLPs for 15 min (Figure 4A,B), 30 min (Figures 2 and 3), or 60 min (Figure 4C,D) at 37 °C, washed three times with 1X PBS, fixed with 4% formaldehyde (10 min at room temperature), and mounted with an antifade reagent (SlowFade Gold). Prior to fixation, cells depicted in Figures 2 and 4 were stained with Hoechst 33342 and either CellTracker Green CMDFA (Figures 2B, C and 4A–D) or CellTracker Violet BMQC (Figure 2A) according to manufacturer's instructions. After fixation, cells depicted in Figure 3 were permeabilized with 0.2% Triton X-100 (5 min at room temperature) and incubated with a blocking agent (Image-iT FX signal enhancer) for 30 min at room temperature. Primary (rabbit pAb against LAMP-1 or mouse mAb against Rab11a) and secondary (Alexa Fluor 488-labeled goat anti-rabbit IgG or Alexa Fluor 647-labeled goat anti-mouse IgG, respectively) antibodies were diluted 1:500 in PBS with 1% BSA and incubated with cells for 1 h at 37 °C; cells were counterstained with DAPI prior to mounting.

Three- and four-color images were acquired using a Zeiss LSM510 META (Carl Zeiss MicroImaging, Inc.; Thornwood, NY) operated in Channel mode of the LSM510 software; a 63X, 1.4-NA oil immersion objective was employed in all imaging. Typical laser power settings were 30% transmission for the 405-nm diode laser, 5% transmission (60% output) for the 488-nm argon laser, 100% transmission for the 543-nm HeNe laser, and 85% transmission for the 633-nm HeNe laser. Gain and offset were adjusted for each channel to avoid saturation and were typically maintained at 500–700 and −0.1, respectively; 8-bit z-stacks with 1024×1024 resolutions were acquired with a 0.7 to 0.9-μm optical slice. LSM510 software was used to overlay channels and to create 3D projections of z-stack images. Images in Figures 2B, C, 3, and 4 are collapsed projections. Pearson's correlation coefficients were determined using SlideBook software (Intelligent Imaging Innovations, Inc.; Philadelphia, PA).

The seven-color image (Figure 2A) was acquired using a Zeiss LSM510 META operated in lambda mode of the LSM510 software; a 63X, 1.4-NA objective was used. Spectral information was acquired over the entire range of the system (411.3-nm to 753.7-nm with a 10.7-nm step) and collected across the 32 PMTs. Laser power and gain were adjusted to avoid saturating the brightest components of the sample. The following settings were used to acquire 8-bit, 1024×1024 z-stacks: 14% transmission for the 405-nm diode laser, 3% transmission (60% output) for the 488-nm argon laser, 3% transmission for the 543-nm HeNe laser, and 3% transmission for the 633-nm HeNe laser; the gain was 850, the offset was −0.15, the optical slice was 0.10 μm, and the frame size was 100 μm^2. Control spectra used for unmixing were acquired using singly labeled control samples. Images were unmixed using the advanced linear unmixing algorithm of the LSM510 software. The brightness and contrast of all channels in the unmixed images were adjusted equally (using the LSM510 software) to balance the intensity between channels. The image in Figure 2A is a collapsed projection.

Cytotoxicity of Drug-Loaded VLPs. MDR was induced in parental Hep3B *via* exposure to increasing concentrations of DOX (25, 50, 75, 100, 150, 200, and 250 nM) in 24-h intervals, interspersed

with 48-h recovery periods during which cells were incubated in complete growth medium without DOX.[41] MDR1$^+$ Hep3B cells were exposed to 1 μM of CsA for 72 h to reverse Pgp-mediated resistance to DOX.[21]

The concentrations of DOX and DOX-loaded VLPs necessary to kill 50% of MDR1$^+$ Hep3B (LC_{50} values—see Figure 6A) were determined by continually exposing 1×10^6 cells/mL to various DOX concentrations for 24 h at 37 °C; the same procedure was used to determine LC_{50} values for free cisplatin and 5-FU. LC_{50} values of the DOX, cisplatin, and 5-FU cocktail and of VLPs loaded with the drug cocktail were determined by continually exposing MDR1$^+$ Hep3B (1×10^6 cells/mL) to various DOX concentrations, in the presence of an equimolar amount of cisplatin and a 3-fold molar excess of 5-FU, for 24 h at 37 °C. Cells were washed three times in 1X PBS (cells that remained adherent were harvested *via* gentle shaking in 5 mM EDTA for 30 min at 37 °C) and stained with SYTOX Green nucleic acid stain and Alexa Fluor 647-labeled annexin V per manufacturer's instructions. The numbers of viable (double-negative) and non-viable (single- or double-positive) cells were determined using a FACSCalibur flow cytometer. SYTOX Green fluorescence was excited by the 488-nm laser and collected in the FL-1 channel (530/30 filter/bandpass), while Alexa Fluor 647 fluorescence was excited by the 633-nm laser and collected in the FL-3 channel (670-nm long pass filter). Curves of DOX concentration *versus* the percentage of viable cells were generated, and GraphPad Prism (GraphPad Software, Inc.; La Jolla, CA) was used to calculate LC_{50} values. The data depicted in Figure 6B were collected by continually exposing 1×10^6 cells/mL of MDR1$^+$ Hep3B or hepatocytes to 285 nM of DOX, the drug cocktail, DOX-loaded VLPs, or VLPs loaded with the cocktail for 24 h or 7 days at 37 °C; the percentage of viable cells in each population was determined as described above. Plots were generated using Sigma Plot, version 11.0 (Systat Software, Inc.; San Jose, CA).

Cytotoxicity of siRNA-Loaded VLPs. The time-dependent viability of Hep3B and hepatocytes exposed to SP94-targeted, siRNA-loaded VLPs (Figure 7A) was determined by exposing 1×10^6 cells to a 1000-fold excess of VLPs for various periods of time (0, 12, 24, 36, 48, 72, 96, and 120 h) at 37 °C. VLPs were loaded with a siRNA cocktail that silences expression of cyclin A2, cyclin B1, cyclin D1, and cyclin E1; 1.1×10^9 particles/mL of VLPs corresponds to a total siRNA concentration of ~150 pM. Cells were washed three times in 1X PBS to remove excess VLPs (cells that remained adherent were harvested *via* gentle shaking in 5 mM EDTA for 30 min at 37 °C) and stained with Alexa Fluor 488-labeled annexin V and propidium iodide per manufacturer's instructions. The numbers of cells in the early (positive for annexin V) and late (double-positive for annexin V and propidium iodide) stages of apoptosis were determined using a FACSCalibur flow cytometer. Alexa Fluor 488 fluorescence was excited by the 488-nm laser and collected in the FL-1 channel (530/30 filter/bandpass), and propidium iodide fluorescence was excited by the 488-nm laser and collected in the FL-2 channel (585/42 filter/bandpass). The total number of apoptotic cells was obtained by adding the numbers of cells in the early and late stages of apoptosis.

The numbers of proliferating and G_0/G_1 arrested Hep3B cells (Figure 7B) were determined by first exposing 1×10^6 cells to SP94-targeted, siRNA-loaded VLPs for various periods of time (same as above) at 37 °C; VLPs were loaded with a siRNA cocktail specific for cyclin A2, cyclin D1, and cyclin E1, and the total siRNA concentration was maintained at ~150 pM. Cells were washed three times in 1X PBS to remove excess VLPs. To determine the percentage of proliferating Hep3B, VLP-treated cells were incubated with 10 μM BrdU (in complete growth medium) for 12 h at 37 °C, harvested by gentle shaking in 5 mM EDTA for 30 min at 37 °C, and fixed with 4% formaldehyde for 30 min at 4 °C. Cells were then washed three times in 1X PBS with 0.1% Triton X-100; incubated in 1 N HCl for 10 min on ice; incubated in 2 N HCl for 10 min at room temperature and then 20 min at 37 °C; incubated in 0.1 M borate for 12 min at room temperature; and washed three times in 1X PBS with 0.1% Triton X-100. Cells were blocked in 1X PBS with 0.1% Triton X-100, 1 M glycine, and 5% goat serum for 1 h at room temperature and then incubated with an Alexa Fluor 488-labeleled mouse monoclonal antibody to BrdU (1:100 dilution in 1X PBS with 1% BSA) overnight at 4 °C. Cells were washed three times with 1X PBS, and the number of cells positive for BrdU incorporation was determined using a FACSCalibur flow cytometer. Cells were considered positive if their mean fluorescence intensities (MFI) were 100 fluorescence units (FU) greater than the MFI of unlabeled cells. To determine the percentage of G_0/G_1 arrested Hep3B, VLP-treated cells were incubated with 1 μg/mL of Hoechst 33342 for 15 min at 37 °C, washed three times with 1X PBS, and immediately analyzed using a MoFlo High Performance Cell Sorter (Dako-Cytomation; Carpinteria, CA) equipped with Dako-Cytomation's SUMMIT software, version 4.3.01. Cells were detected using a 488-nm Innova 90 laser (Coherent Inc.; Santa Clara, CA), and a gate was placed on the forward scatter-side scatter plot that excluded cellular debris. Hoechst 33342 was excited with a 355-nm Innova 90 laser, and emission intensity was collected in the FL-6 channel (450/65 filter/bandpass). Single cells were gated using width and area parameters; the area parameter histogram was used to determine the percentage of gated cells in G_0/G_1, S, and G_2/M phases. Data were acquired with the SSC channel in log mode and all other channels in linear mode.

The concentrations of siRNA-loaded VLPs necessary to silence 90% of cyclin A2, cyclin B1, cyclin D1, and cyclin E1 protein expression (IC_{90} values; see Figure 7C for dose−response curves) were determined by continually exposing 1×10^6 cells/mL to various concentrations (7.1×10^6 to 7.1×10^{10} particles/mL, which corresponds to 1 pM−10 nM of siRNA) of VLPs, loaded with a single type of siRNA, for 48 h at 37 °C. Cells were washed three times with 1X PBS to remove excess VLPs, harvested *via* gentle shaking in 5 mM EDTA (30 min at 37 °C), fixed with 4% formaldehyde (10 min at room temperature), permeabilized with 0.2% Triton X-100 (5 min at room temperature), and exposed to a blocking buffer (1X PBS with 5% BSA) for 1 h at 37 °C. Mouse monoclonal antibodies against human cyclin A2, cyclin B1, cyclin D1, and cyclin E1 (1 μg/μL) were labeled with Alexa Fluor 488 per manufacturer's instructions, diluted 1:500 in 1X PBS with 1% BSA, and incubated with permeabilized cells overnight at 4 °C. Cells were washed three times with 1X PBS and analyzed using a FACSCalibur flow cytometer. Initial concentrations of cyclin A2, cyclin B1, cyclin D1, and cyclin E1 were determined by staining untreated cells (*i.e.*, not previously exposed to siRNA) with anti-cyclin antibodies, as described above; the percentages of initial cyclin concentrations were then determined by dividing the MFIs of siRNA-treated cells by the MFI of untreated cells. GraphPad Prism (GraphPad Software, Inc.; La Jolla, CA) was used to calculate IC_{90} values from the dose−response curves shown in Figure 7A. Lipoplexes composed of cyclin-specific siRNA and the commercially available transfection reagent, Lipofectamine RNAiMAX (LFA), were prepared according to manufacturer's instructions and employed as controls. Empty SP94-targeted VLPs, nontargeted, siRNA-loaded VLPs, and siRNA alone were also tested for their ability to silence expression of various cyclins in Hep3B and hepatocytes (see Figure 8). The time-dependent decrease in cyclin A2, cyclin B1, cyclin D1, and cyclin E1 concentrations induced by siRNA-loaded, SP94-targeted VLPs (Figure 7D) was determined by incubating 1×10^6 Hep3B cells with a 1000-fold excess of VLPs (1.1×10^9 particles/mL of VLPs ≈ 150 pM of siRNA) for various periods of time (0, 12, 24, 36, 48, 72, 96, and 120 h) at 37 °C; VLPs were loaded with a single type of siRNA. Cells were washed, fixed, permeabilized, and stained with Alexa Fluor 488-labeled anti-cyclin antibodies as described above. The dose- and time-dependent decreases in cyclin A2 mRNA (Figures 7C,D, respectively) were determined by incubating Hep3B cells with SP94-targeted VLPs, loaded with the cyclin A2-specific siRNA, as described above. Cells were washed three times with cold 1X PBS to remove excess VLPs; mRNA was isolated from cells and converted to cDNA using the TaqMan Fast Cells-to-CT Kit. Quantitative PCR was performed by SeqWright, Inc. (Houston, TX). Plots were generated using Sigma Plot, version 11.0 (Systat Software, Inc.; San Jose, CA).

Cytotoxicity of Ricin Toxin A-Chain (RTA)-Loaded VLPs. The percentages of Hep3B and hepatocytes that become positive for caspase-3 activation upon exposure to RTA-loaded, SP94-targeted VLPs

were determined by continually incubating 1×10^6 cells/mL with either (1) various concentrations of VLPs (2.0×10^4 to 2.0×10^{10} particles/mL, which corresponds to 1 fM−1 nM of RTA) for 48 h at 37 °C (Figure 9A) or (2) 2.0×10^6 VLPs ([RTA] = ~100 fM) for various periods of time (0, 12, 24, 36, 48, 72, 96, or 120 h) at 37 °C (Figure 9B). Cells were washed three times with 1X PBS to remove excess VLPs (cells that remained adherent were harvested *via* gentle shaking in 5 mM EDTA for 30 min at 37 °C), stained with a CaspGLOW Fluorescein Active Caspase-3 Staining Kit per manufacturer's instructions, and immediately analyzed using a FACSCalibur flow cytometer. Fluorescein fluorescence was excited by the 488-nm laser and collected in the FL-1 channel (530/30 filter/bandpass). Cells were considered positive for caspase-3 activation if their mean fluorescence intensities (MFIs) were more than 100 fluorescent units greater than the MFI of untreated cells (stained with the CaspGLOW kit as described above). RTA-loaded VLPs modified with the SP94 peptide alone or with both the SP94 and H5WYG peptides, as well as RTA alone were employed as controls (Figure 10B). Cells were treated with chloroquine (20 μg/mL) for 24 h at 37 °C to inhibit lysosomal acidification.

The dose- and time-dependent decrease in protein biosynthesis that results upon incubation of Hep3B or hepatocytes with RTA-loaded, SP94-targeted VLPs was determined by continually exposing 1×10^6 cells/mL to either (1) various concentrations of VLPs (2.0×10^4 to 2.0×10^{10} particles/mL, which corresponds to 1 fM−1 nM of RTA) for 48 h at 37 °C (Figure 9C) or (2) 2.0×10^6 VLPs ([RTA] = ~100 fM) for various periods of time (0, 12, 24, 36, 48, 72, 96, or 120 h) at 37 °C (Figure 9D). Cells were washed three times with 1X PBS to remove excess VLPs, harvested *via* gentle shaking in 5 mM EDTA (30 min at 37 °C), stained with a Click-iT AHA Alexa Fluor 488 Protein Synthesis Assay per manufacturer's instructions, and immediately analyzed using a FACSCalibur flow cytometer. Alexa Fluor 488 fluorescence was excited by the 488-nm laser and collected in the FL-1 channel (530/30 filter/bandpass). Initial levels of nascent protein synthesis were determined by staining untreated cells with the Click-iT assay as described above. RTA-loaded VLPs modified with the R8 peptide, empty VLPs modified with either SP94 or R8, nontargeted, RTA-loaded VLPs, and RTA alone were used as controls (Figure 10A). GraphPad Prism (GraphPad Software, Inc.; La Jolla, CA) was used to calculate IC_{90} values from the dose−response curves shown in Figure 9C. Plots were generated using Sigma Plot, version 11.0 (Systat Software, Inc.; San Jose, CA).

Acknowledgment. This work was supported by the NIH/Roadmap for Medical Research under Grant PHS 2 PN2 EY016570B; NCI Cancer Nanotechnology Platform Partnership Grant U01CA151792-01; Air Force Office of Scientific Research Grants FA 9550-07-1-0054/9550-10-1-0054; the U.S. Department of Energy, Office of Basic Energy Sciences, Division of Materials Sciences and Engineering; Sandia National Laboratories' Laboratory Directed Research and Development (LDRD) program; and NIH grant R01 GM42901. Rebecca Lee provided guidance for imaging protocols, Tamara Howard performed electron microscopy, and Mona Aragon created schematics. C.E.A. was supported by IGERT Fellowship Grant NSF DGE-0504276 and by Sandia National Laboratories' Truman Fellowship in National Security Science and Engineering. E.C.C. was supported by NSF IGERT Grant DGE-0549500. M.B. was supported by NSF Nanoscience and Microsystems REU program (Grant DMR-0649132) at the University of New Mexico Center for Micro-engineered Materials. Some images in this paper were generated in the University of New Mexico Cancer Center Fluorescence Microscopy Facility supported by NCRR, NSF, and NCI as detailed at http://hsc.unm.edu/crtc/microscopy/Facility.html. Data was generated in the Flow Cytometry Shared Resource Center supported by the University of New Mexico Health Sciences Center and the University of New Mexico Cancer Center. Sandia National Laboratories is a multiprogram laboratory operated by Sandia Corporation, a wholly owned subsidiary of Lockheed Martin Company, for the United States Department of Energy's National Nuclear Security Administration under Contract DE-AC04-94AL85000.

REFERENCES AND NOTES

1. Peer, D.; Karp, J. M.; Hong, S.; FarokHzad, O. C.; Margalit, R.; Langer, R. Nanocarriers as an Emerging Platform for Cancer Therapy. *Nat. Nanotechnol.* **2007**, *2*, 751–760.
2. Peabody, D. S.; Manifold-Wheeler, B.; Medford, A.; Jordan, S. K.; do Carmo Caldeira, J.; Chackerian, B. Immunogenic Display of Diverse Peptides on Virus-like Particles of RNA Phage MS2. *J. Mol. Biol.* **2008**, *380*, 252–263.
3. Carrico, Z. M.; Romanini, D. W.; Mehl, R. A.; Francis, M. B. Oxidative Coupling of Peptides to a Virus Capsid Containing Unnatural Amino Acids. *Chem. Commun.* **2008**, 1207–1207.
4. Hooker, J. M.; Datta, A.; Botta, M.; Raymond, K. N.; Francis, M. B. Magnetic Resonance Contrast Agents from Viral Capsid Shells: A Comparison of Exterior and Interior Cargo Strategies. *Nano Lett.* **2007**, *7*, 2207–2210.
5. Kovacs, E. W.; Hooker, J. M.; Romanini, D. W.; Holder, P. G.; Berry, K. E.; Francis, M. B. Dual-Surface-Modified Bacteriophage MS2 as an Ideal Scaffold for a Viral Capsid-Based Drug Delivery System. *Bioconjugate Chem.* **2007**, *18*, 1140–1147.
6. Tong, G. J.; Hsiao, S. C.; Carrico, Z. M.; Francis, M. B. Viral Capsid DNA Aptamer Conjugates as Multivalent Cell-Targeting Vehicles. *J. Am. Chem. Soc.* **2009**, *131*, 11174–11178.
7. Wu, M.; Brown, W. L.; Stockley, P. G. Cell-Specific Delivery of Bacteriophage-Encapsidated Ricin A Chain. *Bioconjugate Chem.* **1995**, *6*, 587–595.
8. Wu, M.; Sherwin, T.; Brown, W. L.; Stockley, P. G. Delivery of Antisense Oligonucleotides to Leukemia Cells by RNA Bacteriophage Capsids. *Nanomedicine: NBM* **2005**, *1*, 67–76.
9. Wu, W.; Hsiao, Sonny C.; Carrico, Zachary M.; Francis, Matthew B. Genome-Free Viral Capsids as Multivalent Carriers for Taxol Delivery13. *Angew. Chem., Int. Ed.* **2009**, *121*, 9657–9661.
10. Pickett, G. G.; Peabody, D. S. Encapsidation of Heterologous RNAs by Bacteriophage MS2 Coat Protein. *Nucleic Acids Res.* **1993**, *21*, 4621–4626.
11. Uhlenbeck, O. A Coat for All Sequences. *Nat. Struct. Biol.* **1998**, *5*, 174–176.
12. Bundy, B.; Franciszkowicz, M.; Swartz, J. *Escherichia Coli*-Based Cell-free Synthesis of Virus-like Particles. *Biotechnol. Bioeng.* **2007**, *100*, 28–37.
13. Chackerian, B.; Caldeira, J. d. C.; Peabody, J.; Peabody, D. S. Peptide Epitope Identification by Affinity-Selection on Bacteriophage MS2 Virus-like Particles. *J. Mol. Biol.* **2011**in press.
14. Lo, A.; Lin, C. T.; Wu, H. C. Hepatocellular Carcinoma Cell-Specific Peptide Ligand for Targeted Drug Delivery. *Mol. Cancer Ther.* **2008**, *7*, 579–589.
15. Moore, N. M.; Sheppard, C. L.; Barbour, T. R.; Sakiyama-Elbert, S. E. The Effect of Endosomal Escape Peptides on *in Nitro* Gene Delivery of Polyethylene Glycol-Based Vehicles. *J. Gene Med.* **2008**, *10*, 1134–1149.
16. Jiang, W.; KimBetty, Y. S.; Rutka, J. T.; ChanWarren, C. W. Nanoparticle-Mediated Cellular Response Is Size-Dependent. *Nat. Nanotechnol.* **2008**, *3*, 145–150.
17. Vance, D.; Martin, J.; Patke, S.; Kane, R. S. The Design of Polyvalent Scaffolds for Targeted Delivery. *Adv. Drug Delivery Rev.* **2009**, *61*, 931–939.
18. Weissleder, R.; Kelly, K.; Sun, E. Y.; Shtatland, T.; Josephson, L. Cell-Specific Targeting of Nanoparticles by Multivalent Attachment of Small Molecules. *Nat. Biotechnol.* **2005**, *23*, 1418–1423.
19. Ferrari, M. Nanogeometry: Beyond Drug Delivery. *Nat. Nanotechnol.* **2008**, *3*, 131–132.
20. Lee, J. O.; Lee, K. W.; Oh, D. Y.; Kim, J. H.; Im, S. A.; Kim, T. Y.; Bang, Y. J. Combination Chemotherapy with Capecitabine and Cisplatin for Patients with Metastatic Hepatocellular Carcinoma. *Ann. Oncol.* **2009**, *20*, 1402–1407.
21. Tong, A. W.; Su, D.; Mues, G.; Tillery, G. W.; Goldstein, R.; Klintmalm, G.; Stone, M. J. Chemosensitization of Human Hepatocellular Carcinoma Cells with Cyclosporin A in Post-Liver Transplant Patient Plasma. *Clin. Cancer Res.* **1996**, *2*, 531–539.

22. Shen, X.; Chen, G.; Zhu, G.; Fong, W.-F. (±)-3′-*O*,4′-*O*-Dicynnamoyl-cis-khellactone, a Derivative of (±)-Praeruptorin A, Reverses P-Glycoprotein Mediated Multidrug Resistance in Cancer Cells. *Bioorg. Med. Chem.* **2006**, *14*, 7138–7145.
23. Goren, D.; Horowitz, A. T.; Tzemach, D.; Tarshish, M.; Zalipsky, S.; Gabizon, A. Nuclear Delivery of Doxorubicin *via* Folate-Targeted Liposomes with Bypass of Multidrug-Resistance Efflux Pump. *Clin. Cancer Res.* **2000**, *6*, 1949–1957.
24. Gottesman, M. M.; Fojo, T.; Bates, S. E. Multidrug Resistance in Cancer: Role of ATP-Dependent Transporters. *Nat. Rev. Cancer* **2002**, *2*, 48–58.
25. Masaki, T.; Shiratori, Y.; Rengifo, W.; Igarashi, K.; Yamagata, M.; Kurokohchi, K.; Uchida, N.; Miyauchi, Y.; Yoshiji, H.; Watanabe, S.; Omata, M.; Kuriyama, S. Cyclins and Cyclin-Dependent Kinases: Comparative Study of Hepatocellular Carcinoma *versus* Cirrhosis. *Hepatology* **2003**, *37*, 534–543.
26. Gurzov, E.; Izquierdo, M. Cyclin E1 Knockdown Induces Apoptisis in Cancer Cells. *Neurol. Res.* **2006**, *28*, 493–499.
27. Li, K.; Lin, S.-Y.; Brunicardi, F. C.; Seu, P. Use of RNA Interference to Target Cyclin E-Overexpressing Hepatocellular Carcinoma. *Cancer Res.* **2003**, *63*, 3593–3597.
28. Yuan, J.; Kramer, A.; Matthess, Y.; Yan, R.; Spankuch, B.; Gatje, R.; Knecht, R.; Kaufmann, M.; Strebhardt, K. Stable Gene Silencing of Cyclin B1 in Tumor Cells Increases Susceptibility to Taxol and Leads to Growth Arrest *in Vivo*. *Oncogene* **2005**, *25*, 1753–1762.
29. Franz, D.; David, R.; Jaax, N. D. In *Medical Aspects of Chemical and Biological Warfare*; Sidell, F., Takafuji, E., Franz, D., Eds.; Borden Institute, Walter Reed Army Medical Center: Washington, DC, 1997; pp 631−642.
30. Wu, Y.-H.; Shih, S.-F.; Lin, J.-Y. Ricin Triggers Apoptotic Morphological Changes through Caspase-3 Cleavage of BAT3. *J. Biol. Chem.* **2004**, *279*, 19264–19275.
31. Khalil, I. A.; Kogure, K.; Futaki, S.; Harashima, H. High Density of Octaarginine Stimulates Macropinocytosis Leading to Efficient Intracellular Trafficking for Gene Expression. *J. Biol. Chem.* **2006**, *281*, 3544–3551.
32. Lewis, J. D.; Destito, G.; Zijlstra, A.; Gonzalez, M. J.; Quigley, J. P.; Manchester, M.; Stuhlmann, H. Viral Nanoparticles as Tools for Intravital Vascular Imaging. *Nat. Med.* **2006**, *12*, 354–360.
33. Manchester, M.; Singh, P. Virus-based Nanoparticles (VNPs): Platform Technologies for Diagnostic Imaging. *Adv. Drug Delivery Rev.* **2006**, *58*, 1505–1522.
34. Koudelka, K. J.; Destito, G.; Plummer, E. M.; Trauger, S. A.; Siuzdak, G.; Manchester, M. Endothelial Targeting of Cowpea Mosaic Virus (CPMV) *via* Surface Vimentin. *PLoS Pathog* **2009**, *5*, e1000417.
35. Singh, P.; Destito, G.; Schneemann, A.; Manchester, M. Canine Parvovirus-like Particles, a Novel Nanomaterial for Tumor Targeting. *J. Nanobiotechnol.* **2006**, *4*, 2.
36. Hong, S.; Leroueil, P. R.; Majoros, I. J.; Orr, B. G.; Baker, J. R., Jr.; Banaszak Holl, M. M. The Binding Avidity of a Nanoparticle-Based Multivalent Targeted Drug Delivery Platform. *Chem Biol.* **2007**, *14*, 107–15.
37. Desito, G.; Yeh, R.; Rae, C. S.; Finn, M. G.; Manchester, M. Folic Acid-Mediated Targeting of Cowpea Mosaic Virus Particles to Tumor Cells. *Chem. Biol.* **2007**, *14*, 1152–1162.
38. Hooker, J. M.; Kovacs, E. W.; Francis, M. B. Interior Surface Modification of Bacteriophage MS2. *J. Am. Chem. Soc.* **2004**, *126*, 3718–3719.
39. Anilanmert, B.; Yalcin, G.; Arioz, F.; Dolen, E. The Spectrophotometric Determination of Cisplatin in Urine, Using *o*-Phenylenediamine as Derivatizing Agent. *Anal. Lett.* **2001**, *34*, 113–123.
40. Caldeira, J.; Peabody, D. Stability and Assembly *in Vitro* of Bacteriophage PP7 Virus-like Particles. *J. Nanobiotechnol.* **2007**, *5*, 10.
41. Minko, T.; Kopecková, P.; Kopecek, J. Chronic Exposure to HPMA Copolymer-Bound Adriamycin Does Not Induce Multidrug Resistance in a Human Ovarian Carcinoma Cell Line. *J. Controlled Release* **1999**, *59*, 133–148.